IMAGE ENHANCEMENT TECHNIQUES FOR COCKPIT DISPLAYS

David J. Ketcham, et al

Hughes Aircraft Company

Prepared for:

Office of Naval Research

December 1974

REPORT NO. P74-630R
HAC REF. D0802

CONTRACT N00014-74-C-0313
TECHNICAL REPORT

IMAGE ENHANCEMENT TECHNIQUES FOR COCKPIT DISPLAYS

DECEMBER 1974

AEROSPACE GROUPS
HUGHES
HUGHES AIRCRAFT COMPANY
CULVER CITY, CALIFORNIA

UNCLASSIFIED

SECURITY CLASSIFICATION OF THIS PAGE (When Data Entered)

REPORT DOCUMENTATION PAGE		READ INSTRUCTIONS BEFORE COMPLETING FORM
1 REPORT NUMBER	2. GOVT ACCESSION NO.	3. RECIPIENT'S CATALOG NUMBER
4. TITLE (and Subtitle) Image Enhancement Techniques for Cockpit Displays		5. TYPE OF REPORT & PERIOD COVERED Final Technical Report 4/1/74 - 10/1/74
		6. PERFORMING ORG. REPORT NUMBER P74-530R/D0802
7. AUTHOR(s) David J. Ketcham Roger W. Lowe J. William Weber		8. CONTRACT OR GRANT NUMBER(s) N00014-74-C-0313
9 PERFORMING ORGANIZATION NAME AND ADDRESS Display Systems Laboratory Hughes Aircraft Company Centinela and Teale Sts Culver City, CA 90230		10. PROGRAM ELEMENT, PROJECT, TASK AREA & WORK UNIT NUMBERS NR213-124
11. CONTROLLING OFFICE NAME AND ADDRESS Department of the Navy, Office of Naval Research, Wilson Blvd and N. Quincy St., Arlington, VA 22217		12. REPORT DATE December 1974 13. NUMBER OF PAGES 72
14 MONITORING AGENCY NAME & ADDRESS(if different from Controlling Office)		15. SECURITY CLASS. (of this report) Unclassified 15a. DECLASSIFICATION/DOWNGRADING SCHEDULE

16. DISTRIBUTION STATEMENT (of this Report)

Reproduction in whole or in part is permitted for any purpose of the United States Government.

17. DISTRIBUTION STATEMENT (of the abstract entered in Block 20, if different from Report)

18. SUPPLEMENTARY NOTES

19 KEY WORDS (Continue on reverse side if necessary and identify by block number)

Image Enhancement
Contrast Enhancement
Image Processing

20 ABSTRACT (Continue on reverse side if necessary and identify by block number)

The major objective of this research program was to develop and evaluate three techniques for the real-time enhancement of sensor displays in the airborne cockpit environment.

DD FORM 1 JAN 73 1473 EDITION OF 1 NOV 65 IS OBSOLETE

UNCLASSIFIED

SECURITY CLASSIFICATION OF THIS PAGE (When Data Entered)

20. ABSTRACT

Two enhancement techniques developed and optimized for contrast enhancement are Local Area Brightness and Gain Control (LABGC) and Local Area Histogram Equalization (LAHE). Haar Transform Crispening (HTC) is another technique that was developed and optimized during this program. HTC may be used to sharpen edges in an image which are blurred due to misfocused optics or MTF roll-off.

An evaluation of the enhancement techniques includes subjective evaluations for specific operator tasks and a comparison of mechanization complexities. Photographs of original and enhanced images are included.

Report No. P74-530R

IMAGE ENHANCEMENT TECHNIQUES FOR COCKPIT DISPLAYS

TECHNICAL REPORT

David J. Ketcham
Roger W. Lowe
J. William Weber

Contract No. N00014-74-C0313
Authorization No. NR213-124

December 1974

Prepared for:

Office of Naval Research, Code 211
Department of the Navy
Arlington, Virginia 22217

Prepared by:

Display Systems Laboratory
Hughes Aircraft Company • Culver City, Caliornia 90230

CONTENTS

LIST OF ILLUSTRATIONS

LIST OF ILLUSTRATIONS (Continued)

LIST OF TABLES

1.0 INTRODUCTION

Cockpit display systems are used today to provide pilots and sensor operators with radar, infrared, or television information which is used for navigation, intelligence gathering, target detection, recognition, identification, and designation. In many cases, these tasks require high quality imagery for optimum operator performance. Unfortunately, limitations in the display or sensor system, or both, may lead to degraded performance in meeting mission objectives. Techniques for real time enhancement of sensor imagery show promise for improving operator performance with a minimal increase in system complexity.

1.1 BACKGROUND

Perhaps the most well-known and spectacular examples of image enhancement are those employed to improve pictures transmitted from the moon and planets as part of our space program. In these cases, large computers and long processing times are used to achieve dramatic results by correcting for geometric distortion, eliminating noise, correcting for video non-uniformity across the image, and improving image contrast.

Desirable as these processes may be, their implementation is not feasible in a modern military aircraft. The cockpit environment is one in which processing delays of more than a few milliseconds are not acceptable (this is what is meant by real-time processing) and weight, size, power, and cost must be minimized.

This program has been directed at developing techniques for enhancing sensor imagery to improve the performance of the human operator. A major program objective is the enhancement of sensor images by adjusting the image data to (1) better fit within the performance constraints of the display device or (2) to overcome limitations in sensor performance.

An example of the former is infrared (IR) imagery which has a much larger dynamic range than the cathode-ray tubes on which it is displayed. If an attempt is made to maintain the dynamic range within the limits of the CRT, much information may be lost to the operator because of saturation or compression of the video.

In the second case, the relatively slow response of a FLIR sensor along the scan lines tends to blur edges in the picture, making target recognition and identification more difficult.

1.2 OBJECTIVES

The major objective of this program was to evaluate three image enhancement techniques capable of improving operator performance utilizing sensor display systems. The techniques under evaluation were all judged suitable for implementation and utilization in the cockpit environment. Evaluation was based on subjective analysis of picture quality improvement after the enhancement technique had been applied and on physical data such as complexity and cost. The three techniques that were evaluated are: Local Area Brightness and Gain Control (LABGC), Local Area Histogram Equalization (LAHE), and Haar Transform Crispening (HTC).

1.3 METHODOLOGY

In the performance of this program, four major tasks were performed:

1. Selection, collection, and digitizing of representative sensor data.
2. Development and optimization of the respective enhancement techniques.
3. Processing of the selected images by each of the enhancement processes, and
4. Evaluation of the resulting images.

Representative samples of imagery from each of three major sensor types (IR, TV, Radar) were selected. A flying spot scanner was used to digitize the input image data from photographic transparencies. A digital scan converter was used to capture and digitize frames of raw FLIR sensor data from magnetic video tape. Radar image data was collected directly from computer-compatible digital tapes.

Software for the three enhancement techniques (LABGC, LAHE, and HTC) was developed on the Hughes Real Time System Simulation Facility Sigma 5 digital computer. Each technique was refined to produce the best enhancement possible within real-time cockpit environment constraints. Enhancement parameters such as gain, window size, and filter shapes were empirically adjusted until the resultant images showed the most improvement possible in the opinion of the experimenters.

After the images selected for use in this study were processed, the resulting enhancements were photographically recorded. The photographs (including those of the unprocessed image) were used during the subjective evaluation to determine relative merits of each processing technique.

Subjective evaluation of the processing techniques was accomplished by asking each of ten experienced subjects to rate (on a scale of 1 to 7 with a rating of 4 defined as "normal") the quality of each of the processed images. The rating was applied to a spectrum of operator tasks ranging from vehicle and sensor control through target detection, recognition, and identification. Thus the effectiveness of an enhancement technique could be measured as a function of sensor and task. Further evaluation consisted of designing a tentative hardware mechanization of each technique for estimating complexity.

1.4 SUMMARY

Several conclusions were drawn from this study. All techniques produced the expected observable results in the sensor imagery. Contrast was enhanced and edges in FLIR imagery were indeed sharpened.

The effects of the enhancement processes on improved operator performance were most notable with the contrast enhancement processes applied to FLIR and TV imagery. Although noticeable changes were produced in radar imagery by all enhancement techniques, the subjective evaluations did not indicate that significant improvements in operator performance would be achieved. The evaluation data is inconclusive regarding the effects of these enhancement techniques (LAHE, LABGC, HTC) on radar imagery. Further study in this area is warranted.

It is estimated that LABGC and HTC would be much (by a factor of about 2:1) less complex to implement than LAHE.

In summary, one can conclude from this study that of the three enhancement techniques investigated, local area brightness and gain control offers the potential for significant improvement in performance when applied to electro-optical sensor imagery particularly at mid- and close- ranges. Estimates of hardware complexity suggest that implementation of this technique for use with flight hardware is feasible and well within the state of the art. Further evaluation of this technique through real-time man-in-the-loop simulation or flight test will yield more quantitative data on the cost effectiveness of LABGC in the mission environment.

Subsequent sections of this report contain descriptions of the image collection processes (Section 2.0), detailed discussions of the enhancement techniques (Section 3.0), a presentation of the evaluation results (Section 4.0), and conclusions of the study (Section 5.0).

2.0 IMAGE COLLECTION

The images used in evaluating the various processing techniques were digitized from several sources: radar, FLIR and television. In all cases, the imagery was reduced to a digital format consisting of 256 lines and 256 elements per line. Each picture element, or pixel, was quantized to 6 binary bits representing 64 discrete gray scale levels. This resolution and brightness quantization are sufficient to produce images of adequate quality for evaluation.

The following discusses three devices that were used to digitize images for this study:

1. Flying spot scanner (FSS)
2. Digital scan converter (DSC)
3. Radar direct recording

The FSS device allows the digitization of photographic transparencies. It consists of a cathode ray tube that generates a bright spot whose position is under computer control. This spot is focused onto the image transparency by a lens. The amount of light passing through the transparency at that point is collected by another lens and focused onto a photomultiplier tube (PMT). The PMT output is converted from analog to digital form to produce a digital brightness value as shown in Figure 2-1. This process is repeated until the spot has scanned the entire transparency. The digital numbers collected for each spot on the transparency then make up the digital image. Images are then stored on disk or tape for future processing. Images collected this way are shown in Figures 4-1a, 4-2a and 4-3a.

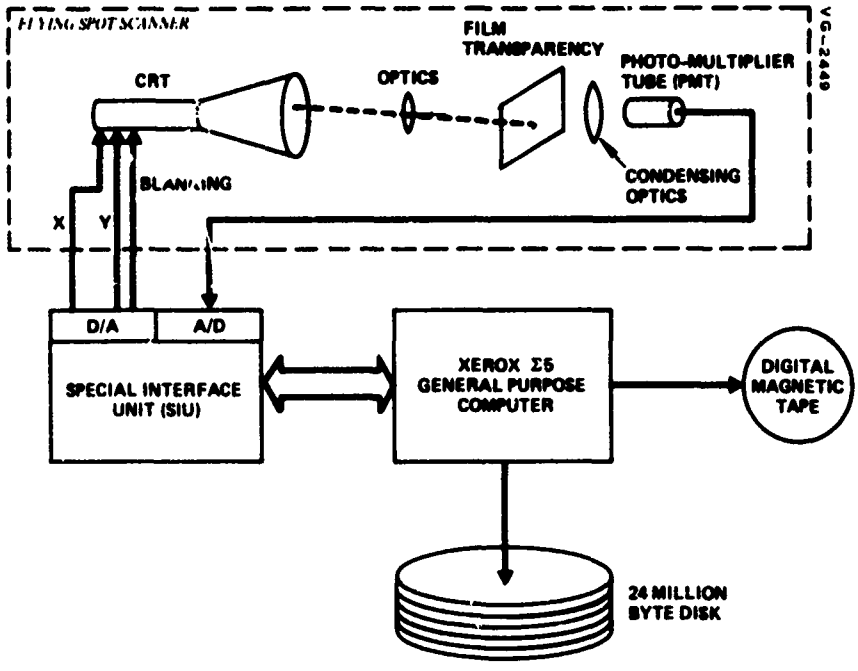

Figure 2-1. Flying spot scanner digitizing process.

The second method of image digitizing is through the use of a digital scan converter (DSC). A DSC is primarily used to buffer information so that sensor video (e.g. radar video), entering at one rate and format, can be output at another. The buffer is a digital memory capable of storing one picture frame. The frame can enter the memory at real-time TV rates and be read out at much slower computer rates. Figure 2-2 illustrates the functional operation of the DSC as it was used to digitize FLIR images from video tape.

The DSC was used to capture single frames from a TV compatible Forward Looking Infrared (FLIR) sensor system. This was done by monitoring the FLIR imagery as it was played on the video tape recorder. Depressing a switch at the monitor caused the desired image to be captured in the DSC memory for subsequent read-out by the computer. The computer then transferred the digital image from the DSC memory to magnetic tape or disc. FLIR scenes captured this way are shown in Figures 4-4a, 4-5a, 4-6a, and 4-7a.

This technique was used because it overcomes some of the problems of digitizing photographs of FLIR displays using the FSS. When using film and a cathode ray tube, information and dynamic range is lost due to limitations in the brightness transfer function or gamma of both the CRT and film.

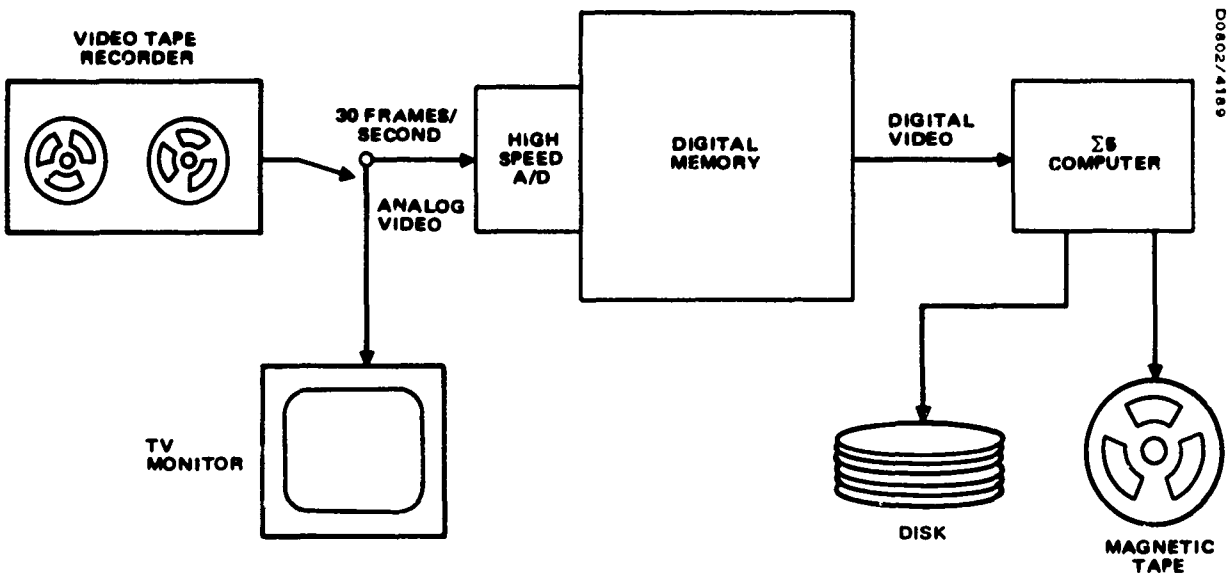

Figure 2-2. Functional operation of the digital scan converter (DSC)

Capturing FLIR images directly from video tape preserves the inherent characteristics of FLIR imagery. The four pictures collected and digitized for this study are typical of FLIR imagery.

The radar images collected for this study were directly recorded on digital magnetic tape during flight test of the Forward Looking Advanced Multi-mode Radar (FLAMR). These tapes are initially wide band recordings that are converted to computer compatible tapes (CCT) on the ground. The images thus recorded are from the radar's doppler beam sharpened mode (DBS) which is similar to a synthetic array type of ground mapping radar. Four scenes were selected that are representative of radar imagery and are shown in Figures 4-8a, 4-9a, 4-10a, and 4-11a.

3.0 ENHANCEMENT TECHNIQUES AND RESULTS

Three image enhancement techniques are described in this section: two contrast enhancement techniques and one resolution enhancement technique. Local Area Brightness and Gain Control (LABGC) and Local Area Histogram Equalization (LAHE) comprise the contrast enhancement techniques. The resolution enhancement is achieved through Haar Transform Crispening (HTC). Each of these will be described in detail.

3.1 LOCAL AREA BRIGHTNESS AND GAIN CONTROL

This section describes a contrast enhancement technique that utilizes two prominent variables of display systems: brightness and gain. These variables help match the image video offset and dynamic range to the display such that the operator can extract the most useful visual information. However, these variables are constant over an entire picture frame. While for the most part this is acceptable, no real enhancement can be achieved by their manipulation. An increase in video gain does increase overall image contrast but detail in dark and light portions saturate due to the limited dynamic range of the display device (usually a CRT). What is needed is a way of increasing the contrast in small areas of an image without causing saturation in other areas. Continuous adjustment of gain and brightness in small areas throughout the picture would achieve this purpose.

Local area brightness and gain control (LABGC) was achieved by sliding a small window through the image and adjusting the center element by gain and brightness. Figure 3-1 depicts this window which was chosen to be 9 pixels by 9 lines. Earlier attempts at LABGC consisted of first adjusting the brightness of the window's center element and then applying a

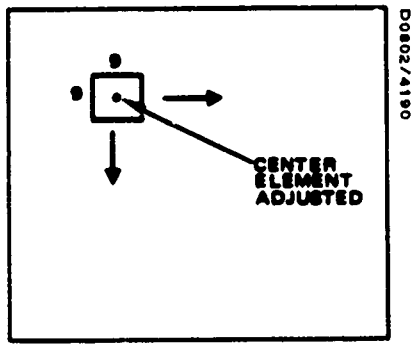

Figure 3-1. Sliding window for local area brightness and gain control.

constant gain factor. This process can be best illustrated by the one-dimensional example of Figure 3-2. Figure 3-2a shows a typical line of video where small detail is present in both the dark and light regions. This example shows 6 bit digital video where 0 is the maximum black and 63 is the maximum white. The first step of the LABGC process, shown in Figure 3-2b, is to adjust the brightness toward mid-gray, which, digitally, is 32. This is done by adding to the center pixel the difference between mid-gray (32) and the average brightness of 9 pixels. Notice that this produces a video which tends to be flat and washed out. However, this step is necessary in order that the applied gain function does not cause saturation. The next step, shown in Figure 3-2c is the application of a gain function to the brightness adjusted video of Figure 3-2b. This is done by multiplying the video by a constant gain uniformly across the line. The two-dimensional visual counterpart of this process is shown by the tank image of Figure 3-3, where a, b, and c correspond to a, b, and c of Figure 3-2. Notice that the processed image tends to take on a binary appearance - there's little mid gray information. A considerable amount of detail has been brought out in the image but it is not pleasing. The obvious way to avoid the binary problem is to decrease the gain factor. Figure 3-4 shows the effect of lower uniform gain. This helps, but it appears desirable to maintain a high gain in some areas of the image while reducing it in others. For example, a lower gain in the grass area would help maintain a grass-like texture but a higher gain in the tread area would help to enhance it.

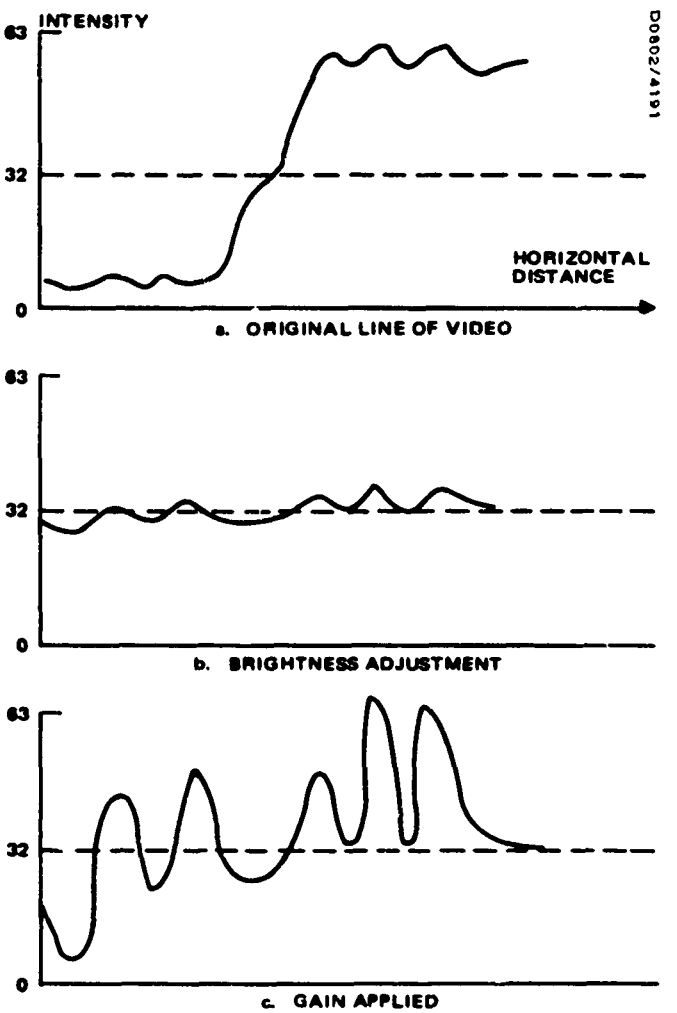

Figure 3-2. One-dimensional example of local brightness and gain control.

a. Original 256 x 256 resolution x 6 bit video.

b. Brightness adjusted.

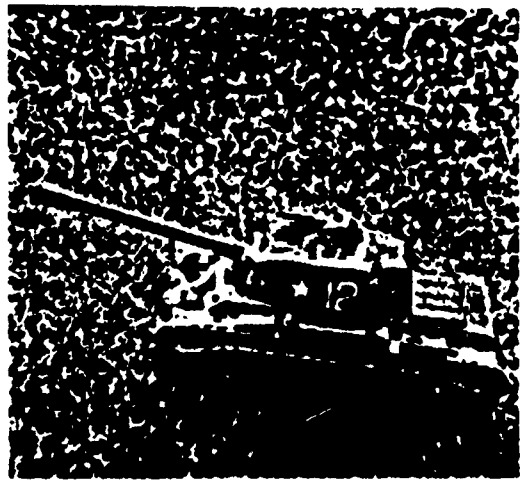

c. Gain = 10 applied.

Figure 3-3. Example of local area brightness and gain control with uniform gain.

DC802/4193

a) gain = 2

b) gain = 3

c) gain = 4

d) gain = 5

Figure 3-4. Effects of differing levels of uniform gain with brightness adjusted toward mid-gray.

This latter effect can be achieved by making the brightness and gain vary as a function of the local statistics within the image. If the gain is a function of the standard deviation of pixel values within the sliding window, then the gain can be made larger in areas with little gray scale level change and smaller in areas of large change. Figure 3-5 illustrates in histogram form the statistics of different local areas of the image. If the gain function applied to the image is inversely proportional to the standard deviation as in Figure 3-6 the desired effect is achieved. One way to apply this gain is about the local statistical mean of the video. But this causes a problem; certain pixels may exceed the bounds of maximum black or maximum white. This problem can be overcome by applying a brightness control to bring the pixel intensities back within bounds. Figure 3-7b illustrates the application of video gain about the local mean to improve contrast. Figure 3-7c shows the application of the brightness control to avoid saturation. The combination of a gain function based on the local standard deviation and a brightness bias control comprise the LABGC contrast enhancement technique.

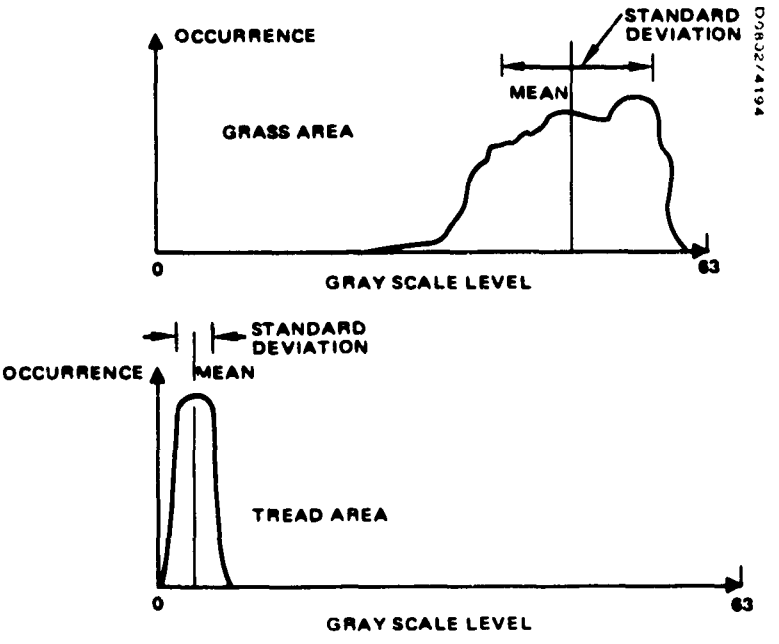

Figure 3-5. Local image statistics.

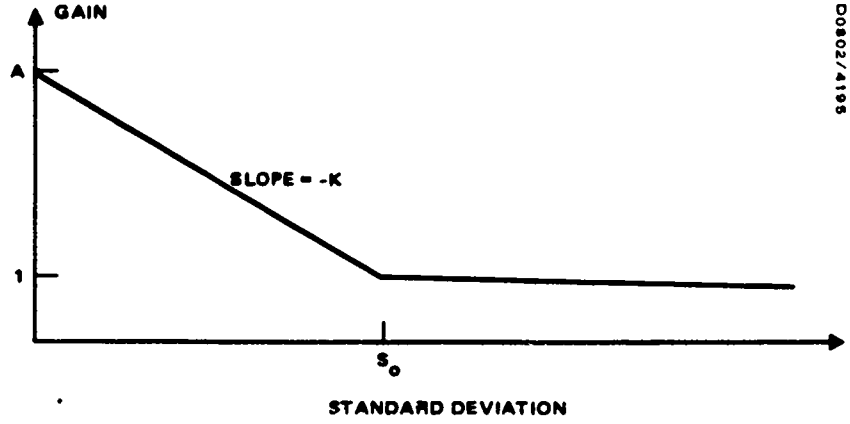

Figure 3-6. Gain as a function of standard deviation within sliding window.

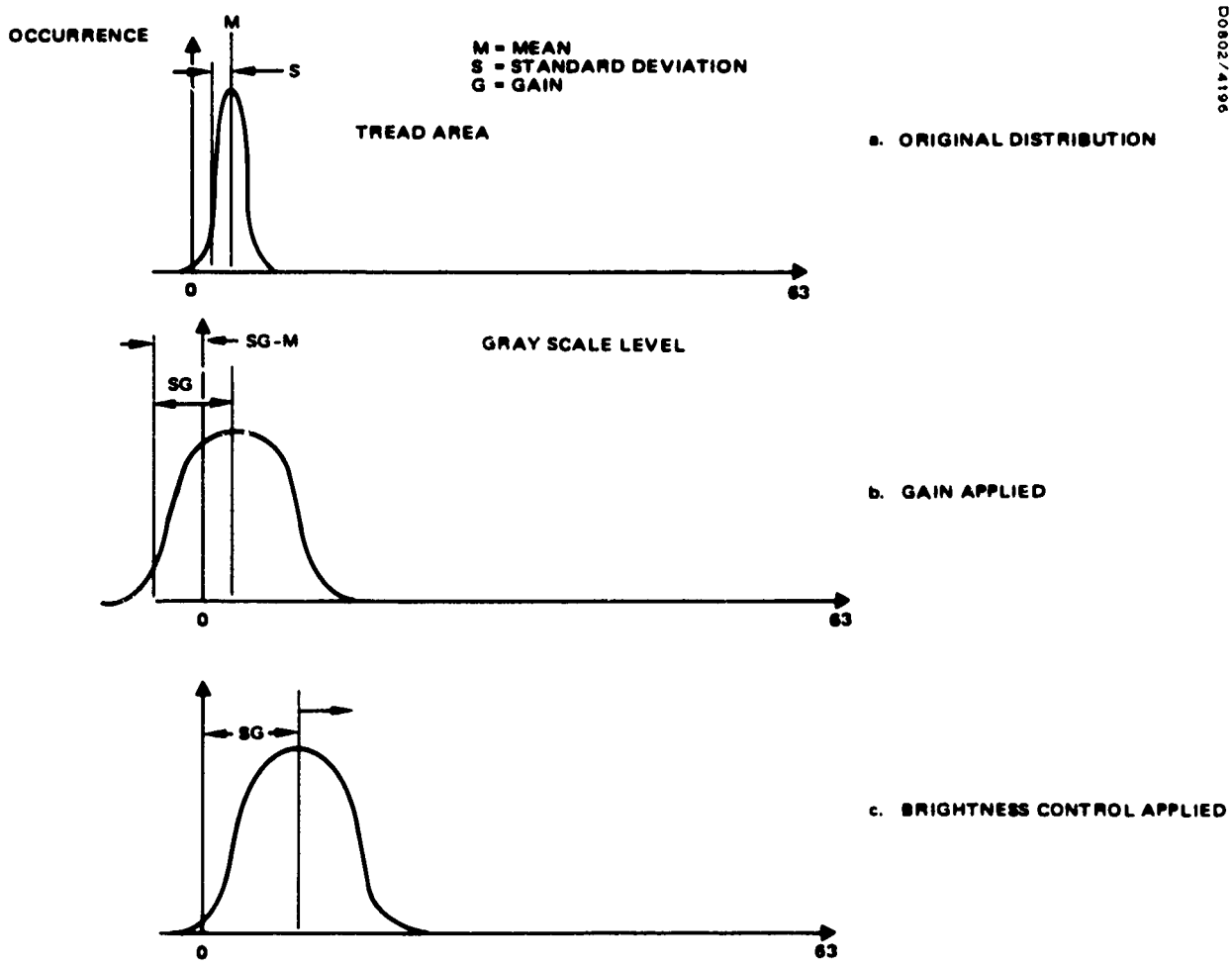

Figure 3-7. Statistical gain and brightness control.

In more mathematical terms, the LABGC technique is described as follows. Within the 9 x 9 sliding window the mean and standard deviation are computed as

$$\text{MEAN} = M = \frac{\sum_{i=1}^{9}\sum_{j=1}^{9} I(i,j)}{81}$$

and

$$\text{STANDARD DEVIATION} = S = \sqrt{\frac{\sum_{i=1}^{9}\sum_{j=1}^{9} I^2(i,j)}{81} - \text{MEAN}^2}$$

where

I (i, j) = a pixel within the sliding window.

Then the gain function as shown in Figure 3-6 is given by

$$\text{GAIN} = G = A - KS$$

where A is the upper limit of the gain, K is the slope of the function, and S is the standard deviation within the window. If G < 1, then G is set to 1.

The computation of the brightness control value is based on the following logic. The majority of the pixels in the sliding window lie within the standard deviation about the mean. Hence, most intensities are bounded by M - S and M + S. This information can be used to determine if the gain adjusted video will exceed the black or white intensity boundaries. Figure 3-7b depicts a situation where maximum black is exceeded after the gain is applied. The value of the brightness bias control for this case is the distance that the video distribution extends beyond 0 or maximum black. Thus the brightness bias is GS - M. Similarly, for the maximum white boundary (63) the brightness bias is given by 63 - (M + GS).

This brightness control logic works well for the majority of video distributions. However, certain distributions arise where the above logic produces picture anomalies. Figure 3-8b has been processed by the LABGC technique using the above brightness control logic. Note the "bordering" that occurs at high contrast edges. In particular, notice the white dot in the black bay area at the center left of the original image (3-8a). In the enhancement (3-8b) a 9 x 9 window anomaly has been produced at this point. Figure 3-9a illustrates in histogram form the statistics of this local area in the original image. When the gain and brightness bias control is applied to the image as in Figure 3-8c the resulting distribution is biased more than necessary to prevent the enhanced pixels from exceeding maximum black as they do in 3-9b. This problem is solved by limiting the brightness bias value when the standard deviation does not accurately represent the video distribution which in this case is to the left of the mean. A better brightness bias value is MG - M which can be seen in Figure 3-9b. For the maximum white limit the bias value using this logic is

$$B = 63 - (M + G(63-M)).$$

If the brightness bias value (B) is computed using a combination of both the mean and standard deviation logic discussed above, then the center element of the sliding window is enhanced as follows,

$$\hat{I}(5,5) = \left[I(5,5) - M\right] * G + B + M$$

where $\hat{I}(5,5)$ is the enhanced center window element. Figure 3-8c shows the results of this combined brightness control logic and a statistical gain.

3.2 LOCAL AREA HISTOGRAM EQUALIZATION

Histogram equalization is a unique image contrast enhancement technique. Historically, it has been applied only to an entire picture frame. This technique is called full-frame histogram equalization (FFHE). What is described here is a procedure for applying histogram equalization to a smaller portion or local area of a picture frame. The advantage of the

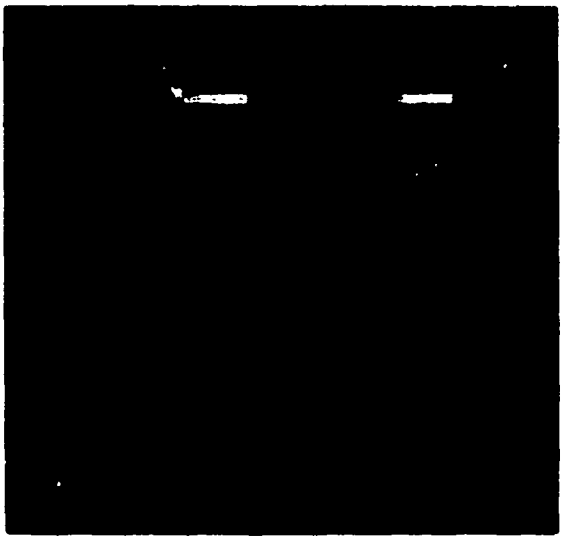

a) Original

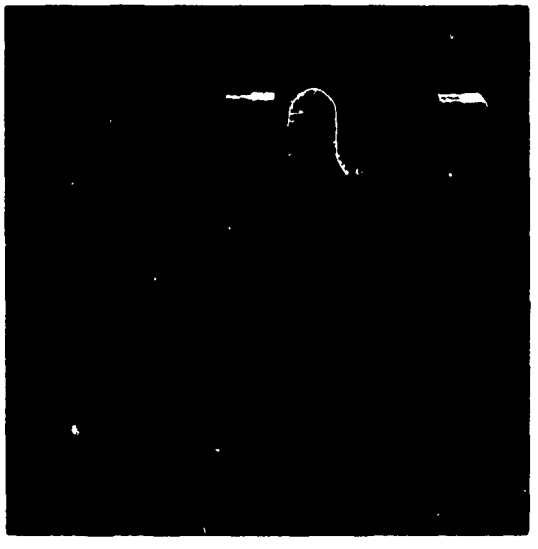

b) LABGC with standard deviation brightness control only

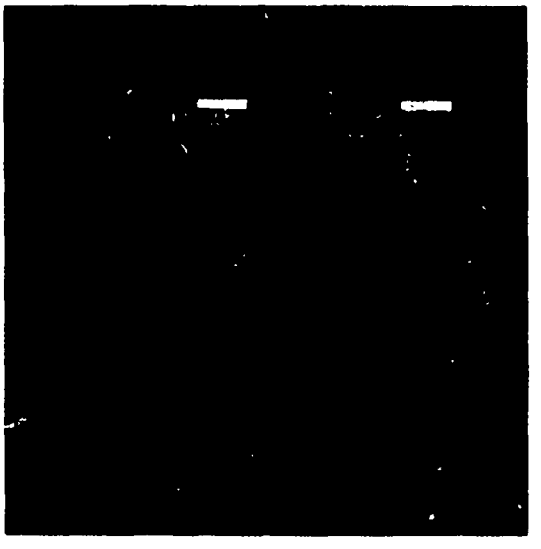

c) LABGC with both standard deviation and mean brightness control

Figure 3-8. Example of "bordering" due to improper brightness control.

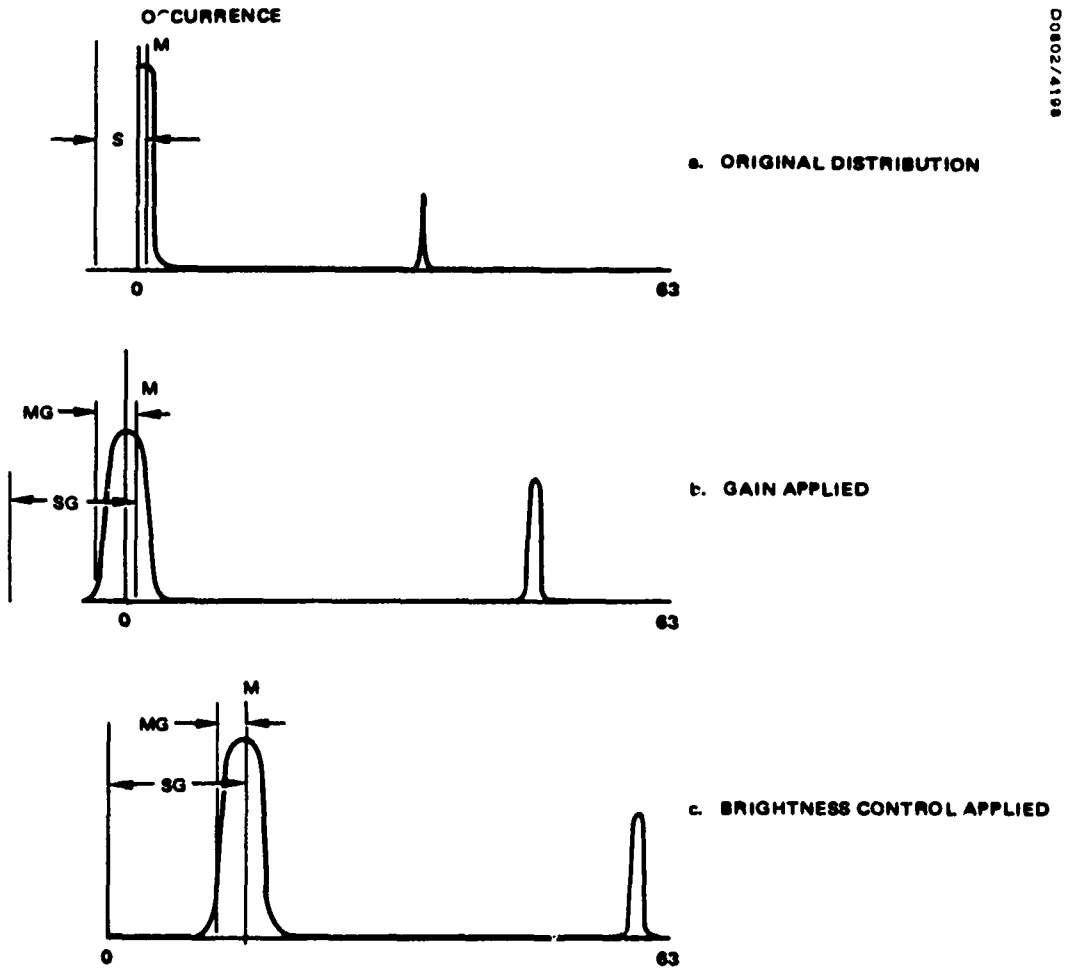

Figure 3-9. Distributions causing "bordering" due to improper brightness control.

local area histogram equalization (LAHE) technique is that it eliminates contrast attenuation in image areas that represent a statistically small but important portion of the gray scale histogram. The following paragraphs review FFHE and then describe the LAHE technique.

An image histogram is formed by accumulating and tabulating the occurrences of each pixel (picture element) intensity. For the example in Figure 3-10, the intensities range over 64 quantized levels. The histogram for the entire image is characterized in Figure 3-11. This distribution indicates that the picture is generally light with few areas in the mid-gray range and some predominantly very dark areas. It shows that the distribution of gray scale information primarily lies at either end of the light/dark

Figure 3-10. 56 x 256 x 6 bit original tank image.

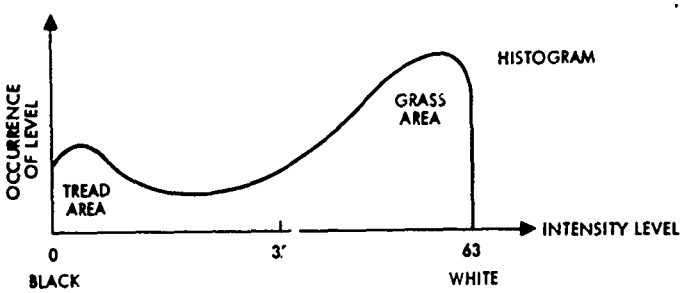

Figure 3-11. Image histogram for Figure 3-10.

intensity scale. Thus, if the image is displayed on a CRT which generates 16 shades of gray, the result is equivalent to slicing the gray scale axis of the histogram into 16 equally spaced levels as shown in Figure 3-12.

It becomes apparent that if the amount of information is related to the level of occurrence of each gray scale then each intensity level in the displayed image does not carry the same amount of information. If the picture intensities are distributed as in Figure 3-11, it might be better to use more display gray scale levels where there are more occurrences of gray scale information in the image and fewer levels where there is less

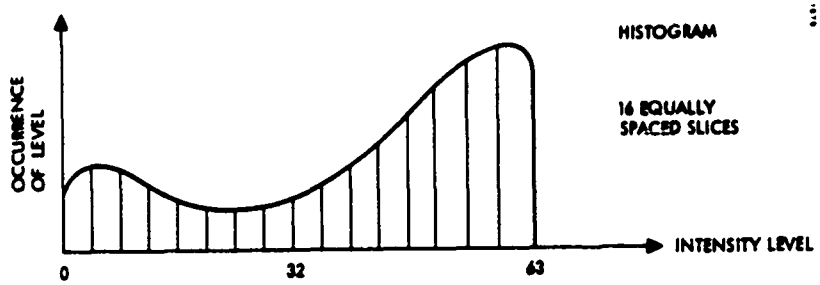

Figure 3-12. Equal intensity level slicing.

data. This nonuniform distribution of gray scale levels can be computed by finding the total area under the histogram and dividing this area into N or, for example, 16 slices having equal areas as shown in Figure 3-13.

The intensity level boundaries for each slice then define the range of original intensity levels that will be assigned a new gray scale level for the displayed image. When this is done a histogram of the resulting displayed image has a flat or equal distribution of gray scale levels as in Figure 3-14. Hence the name "Histogram Equalization."

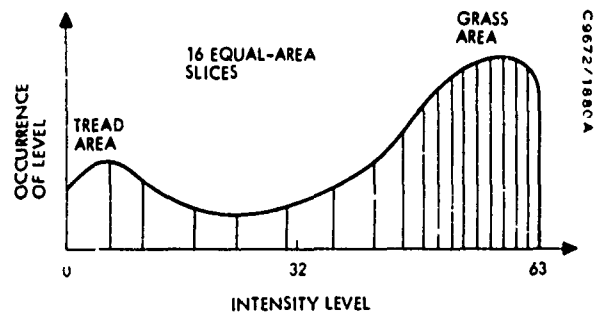

Figure 3-13. Equal area slicing.

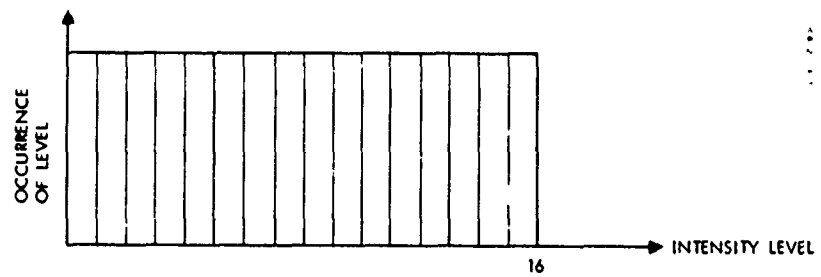

Figure 3-14. Histogram of histogram equalized image.

Figure 3-16 shows the effect of FFHE. The contrast and hence the detail in the light areas of the image, such as the grass and the top of the tank, have been enhanced. The dark areas of the image, mainly around the tread area, have not been enhanced since these brightness levels do not show a high level of occurrence in the histogram. Figure 3-15 helps visualize this effect. Note that the area of the histogram having low occurrence represents a part of the image that will have half as many gray scale levels in a processed picture than in the original. Obviously, if the target of interest lies in that area of the image, FFHE processing would not be an enhancement.

This difficulty can be resolved by using local area histogram equalization. That is, rather than redistributing the gray scale levels based on a histogram representing the entire image, the equalization can be carried out on a two-dimensional sliding window basis. Thus, the intensity for any particular point in the image is adjusted according to a histogram of the area contained within a window immediately surrounding the point as shown in Figure 3-17. In operation, this window moves across the image in two dimensions, horizontally and vertically. These reassigned center picture elements then make up the processed image. On images like the tank, detail is greatly enhanced in regions like the tread rollers as shown in Figure 3-16c.

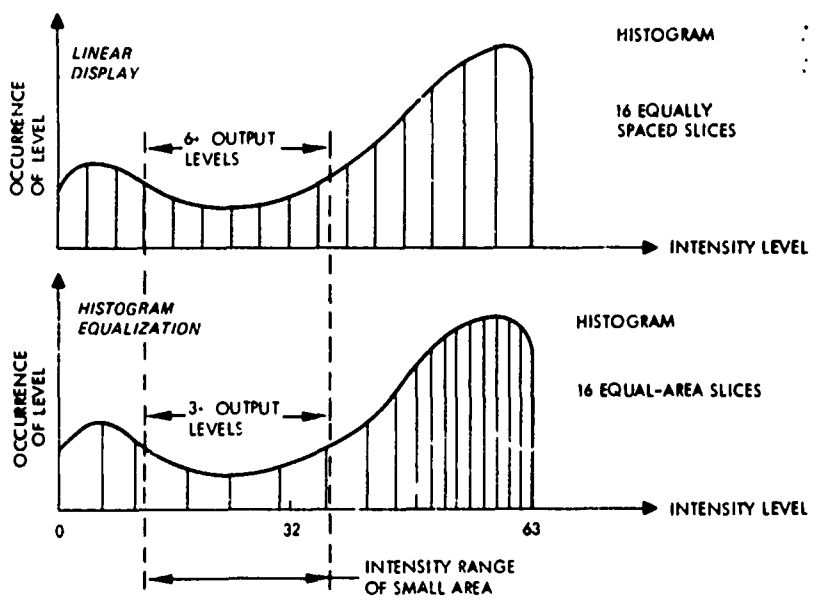

Figure 3-15. Potential deficiency of full frame Histogram equalization.

D0802/4200

a. Original

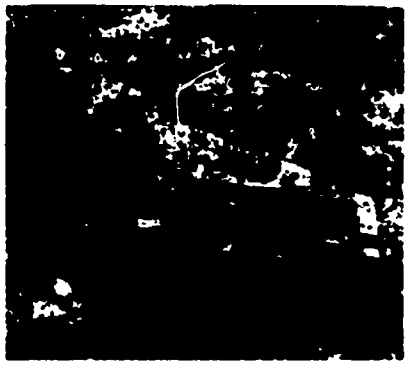

b) Full frame histogram equalized

c) Local area histogram equalized

Figure 3-16. Comparison of full frame and local area histogram equalization.

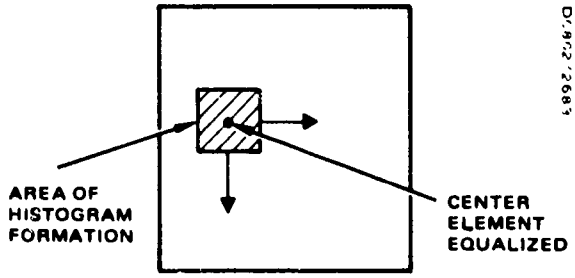

D7802/2683

Figure 3-17. Two-dimensional Histogram equalization.

This process of forming a histogram around each picture element is quite time consuming. It would be more efficient to compute a histogram and equalize a group of picture elements rather than just one. Therefore, a trade-off study was performed to determine the optimum number of elements to equalize within each window area. Based upon the histogram in the sliding window of 32 rows by 32 columns, the picture elements in the center N rows and N columns were adjusted for N = 1, N = 2, N = 4, N = 8, N = 16, and N = 32. Figure 3-18 illustrates these different size inner windows starting in the upper left hand corner of an image. The large outer box is the 32 x 32 window that represents the boundaries of histogram formation. The heavy dotted and cross-hatched areas represent those picture elements that get equalized. The light dotted and lined areas represent the next areas to be equalized. This equalization is based on the histogram formed within the boundaries of the outer dashed box. The results of these differing inner window sizes are shown in Figures 3-19a through 3-19f. Each picture corresponds to the process depicted in Figures 3-18a-f. It can be seen that for N = 8, 16, and 32, the enhanced picture has a "boxy" look while for N = 1, 2, and 4, this effect is absent. Therefore, the conclusion is that the pixels in the center 4 rows and 4 columns of each sliding window can be equalized without undue picture distortion while producing good computational speed.

A potential problem arises in local histogram equalization when the distribution is concentrated at only a few intensities as in Figure 3-20. In this particular example, the intensities run from 29 to 35. After histogram equalization, the intensity distribution would look similar to that in Figure 3-21. Notice that true equalization has not been achieved since the upper brightness levels are not being utilized. This is due to the fact that there are fewer gray scale levels in the area to be enhanced than there are display levels. When this particular situation occurs, the histogram equalization technique enhances the contrast but also biases the equalized video toward the dark end of the intensity scale as shown in Figure 3-21. This problem is alleviated in the following manner. The arithmetic means of intensity levels in the original sliding window area and the histogram equalized

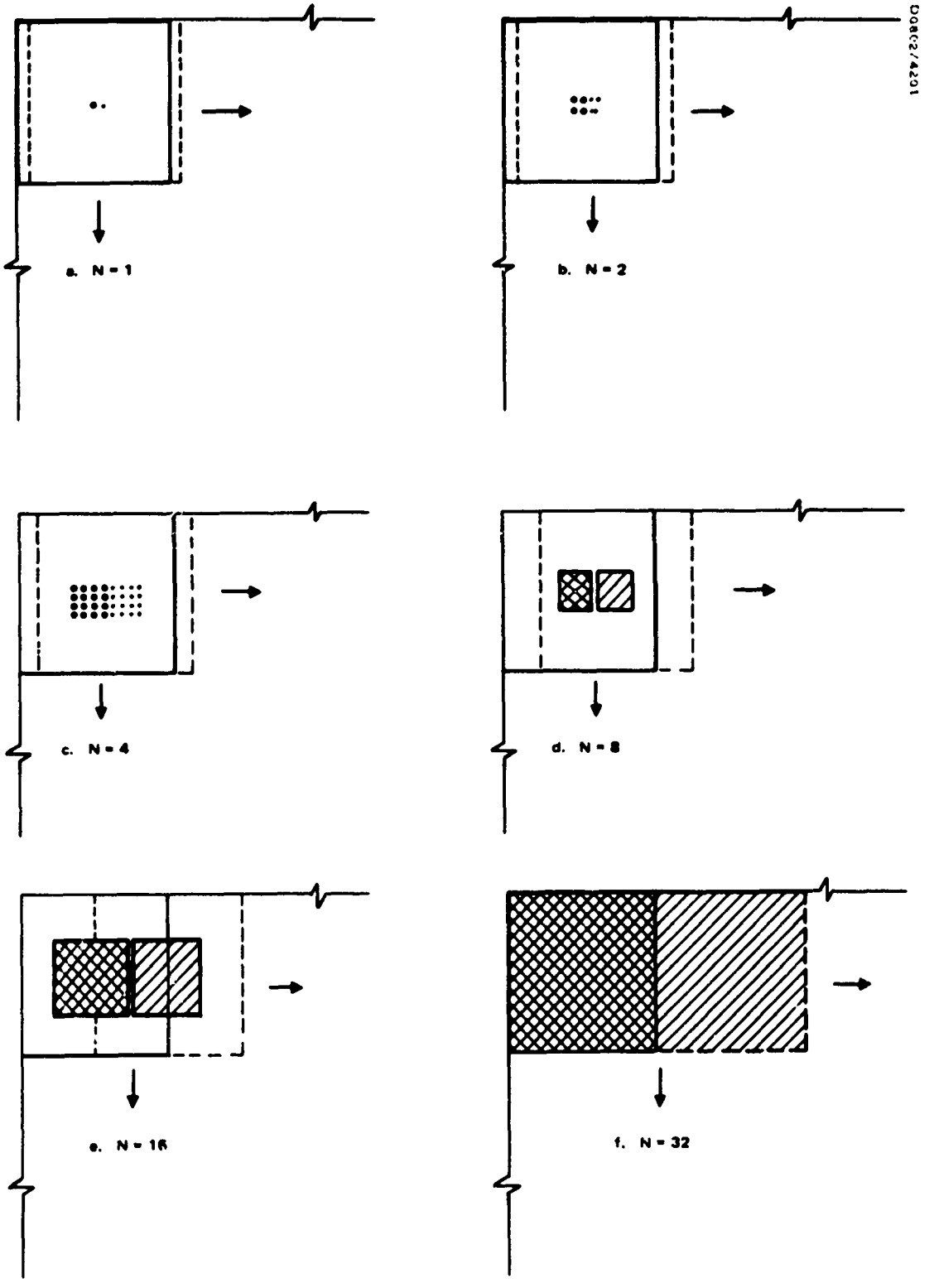

Figure 3-18. Different inner window sizes for the LAHE technique.

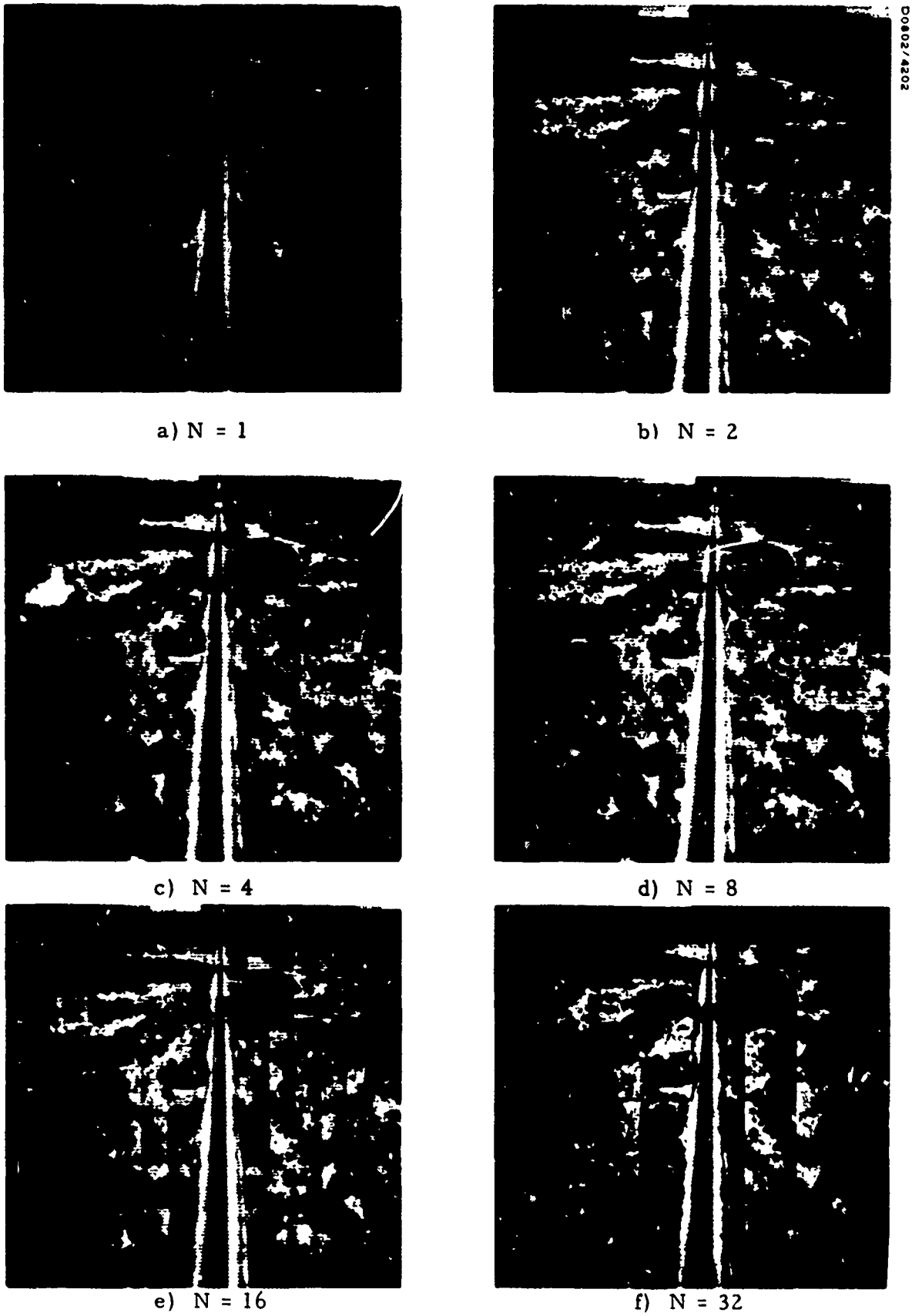

a) N = 1

b) N = 2

c) N = 4

d) N = 8

e) N = 16

f) N = 32

Figure 3-19. Effect of equalizing N^2 picture elements for each local area histogram.

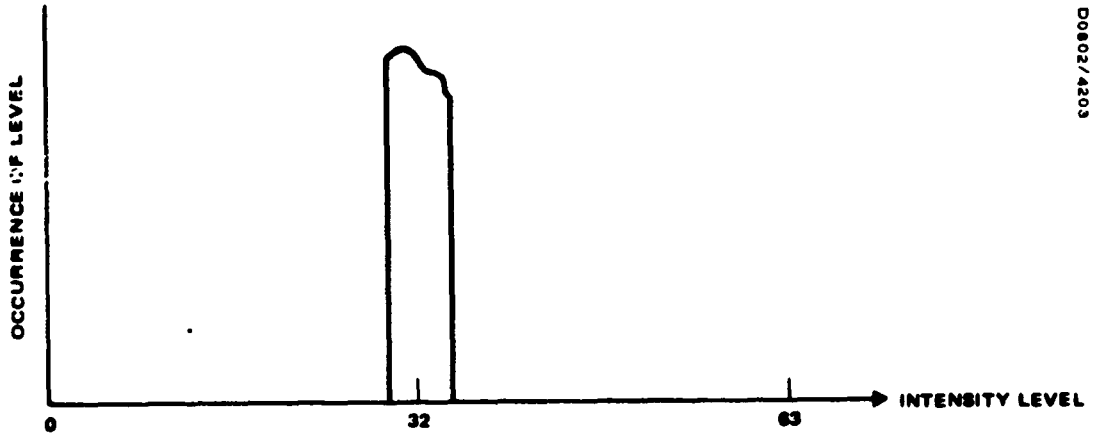

Figure 3-20. Picture histogram within sliding window showing a small range of intensity levels.

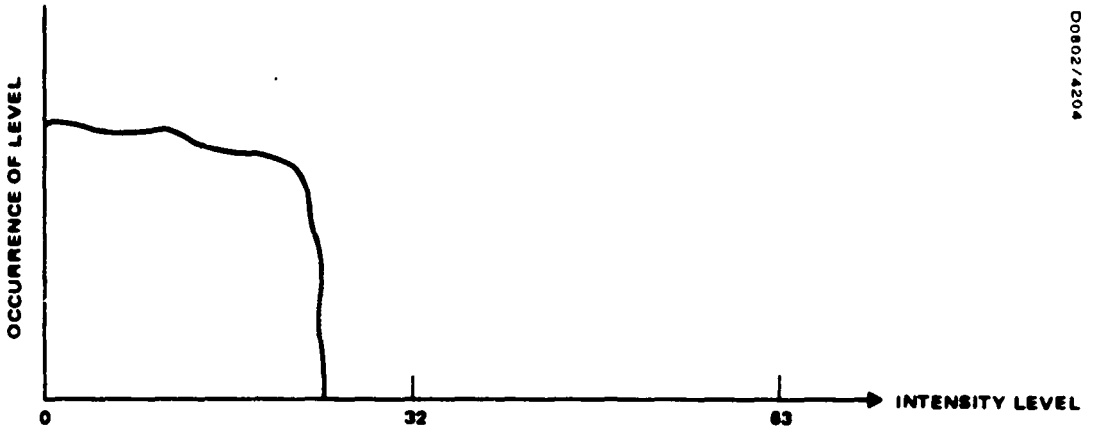

Figure 3-21. Histogram of histogram equalized sliding window of Figure 3-20

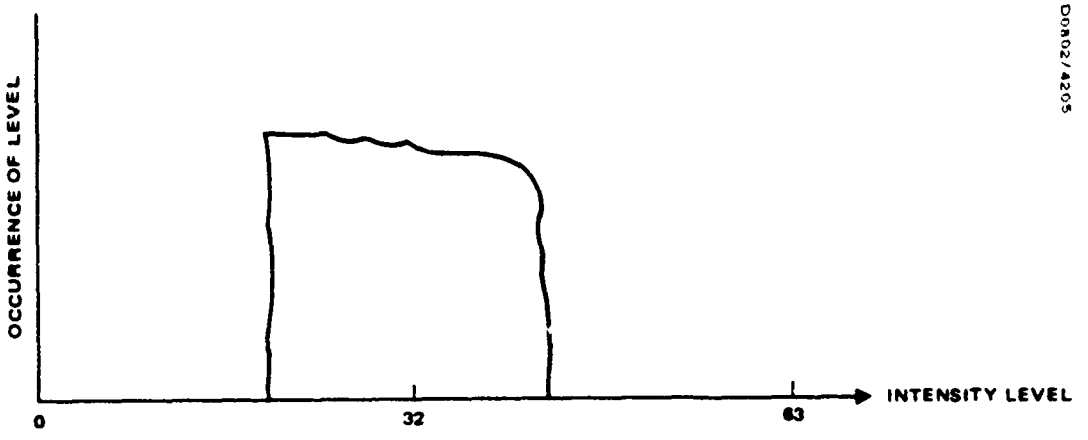

Figure 3-22. Histogram of adjusted histogram equalized sliding window.

data are computed. Based upon these means the histogram equalized intensities are biased to the right to make the two means correspond. In the example above, the mean in the original sliding window is 32 and the mean of the intensity levels after histogram equalization is 14. Therefore, the intensity levels after histogram equalization are biased by 18 so that their mean is now 32 which corresponds to the original mean. The result of this biasing is shown in Figure 3-22. This biasing produces a contrast enhanced image whose mean brightness in local areas is matched to the original.

In summary, the local area Histogram Equalization technique is a powerful one for enhancing image contrast. It does so by the non-linear assignment of gray scale levels in an adaptive manner based upon the local statistics of the image.

3.3 HAAR TRANSFORM FILTERING

Much analysis and experimental work has been done in the general area of spatial frequency filtering of images. What is discussed here is a way of achieving results similar to the Fourier Transform techniques without requiring an actual Fourier Transform. The Haar transform is utilized since it is much faster and easier to compute. Table 3-1 lists various transforms that are currently being used in image processing work. The number of computations required for each transform are enumerated. Notice that the Haar transform requires the fewest number of computations.

TABLE 3-1. IMAGE TRANSFORMS

TRANSFORM	NO. OPERATIONS	N= 512	N= 1024	TYPE OPERATIONS
FOURIER	$2N^3$	268,435,456	2,147,483 648	COMPLEX MULTIPLIES & ADDS
FFT	$2N^2LOG_2N$	4,718,592	20,971,520	COMPLEX MULTIPLIES & ADDS
HADAMARD/WALSH	$2N^2LOG_2N$	4,718,592	20,971,520	ADDS
HAAR	2N(N-1)	523,263	2,095,104	ADDS
CONVOLUTION	N^2XM^2	67,108,864 (M = 16)	1,073,741,824 (M = 32)	MULTIPLIES AND ADDS

VG-2464

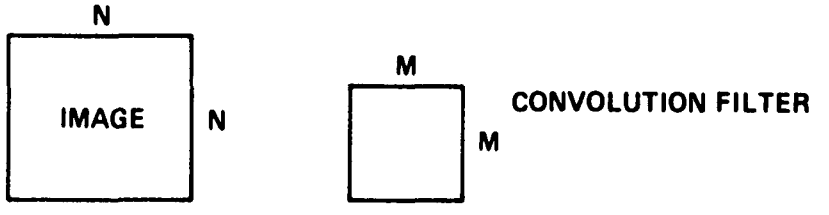

The characteristics of the Haar transform decomposition are not as general and useful as the Fourier and Hadamard. However, the Haar decomposition is characterized by a differential-like breakdown that suggests its use for crispening. Figure 3-23 shows three kernels or basis vectors for a Fourier, Hadamard and rational Haar transform. Note that the rational Haar waveforms contain many zero areas that result in fewer computations. The Fourier transform is composed of both a sine and cosine function. Only the sine waveform is shown in Figure 3-23. Note the magnitudes of the Fourier waveform are generally less than 1. This necessitates complex multiplication rather than simple addition. The Hadamard and rational Haar waveforms on the other hand have magnitudes of only 1, -1 and 0. This results in only addition and substraction for their computation.

The following section describes in detail the derivation of the rational Haar transform. The normal Haar transform is characterized by a matrix that contains entries that are powers of $\sqrt{2}$ which eliminates simple addition and subtraction. The derivation shows how these $\sqrt{2}^n$ terms can be factored out in such a way that only addition and subtraction (1, -1 terms) and weighting factors are required to perform the transform. For a combination of forward and inverse Haar transforms, the weighting factors are simple

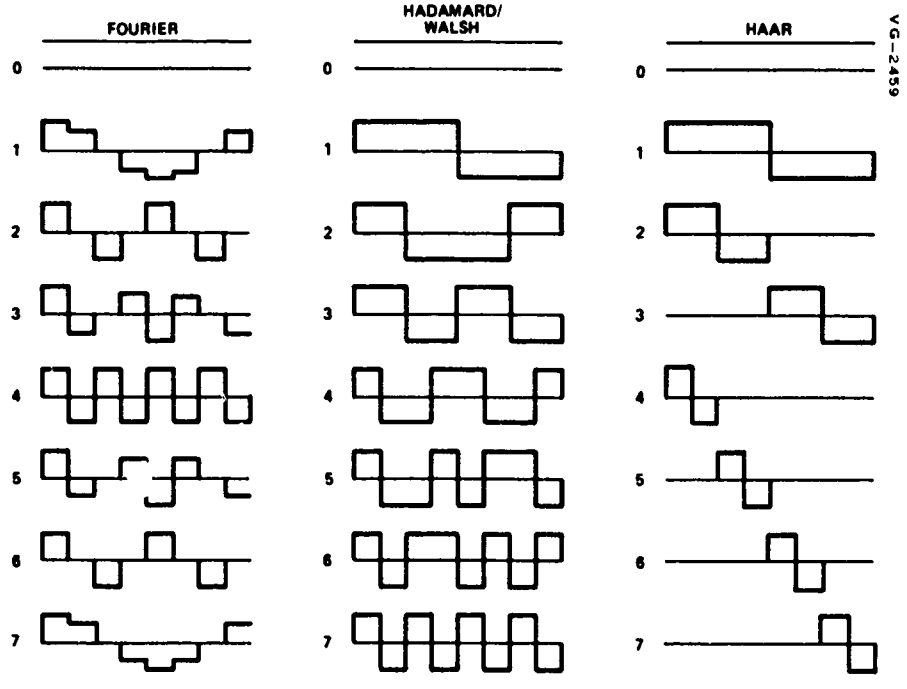

Figure 3-23. 8 point transform decomposition waveforms.

binary shifts. This is an important result for high speed computation. The rational Haar transform matrix can itself be factored into a product of matrices that each contain very simple entries. This matrix product is the basis for the fast Haar transform algorithm depicted in Figure 3-24.

INPUT VECTOR $V = (V_1, V_2, V_3, V_4, V_5, V_6, V_7, V_8)$

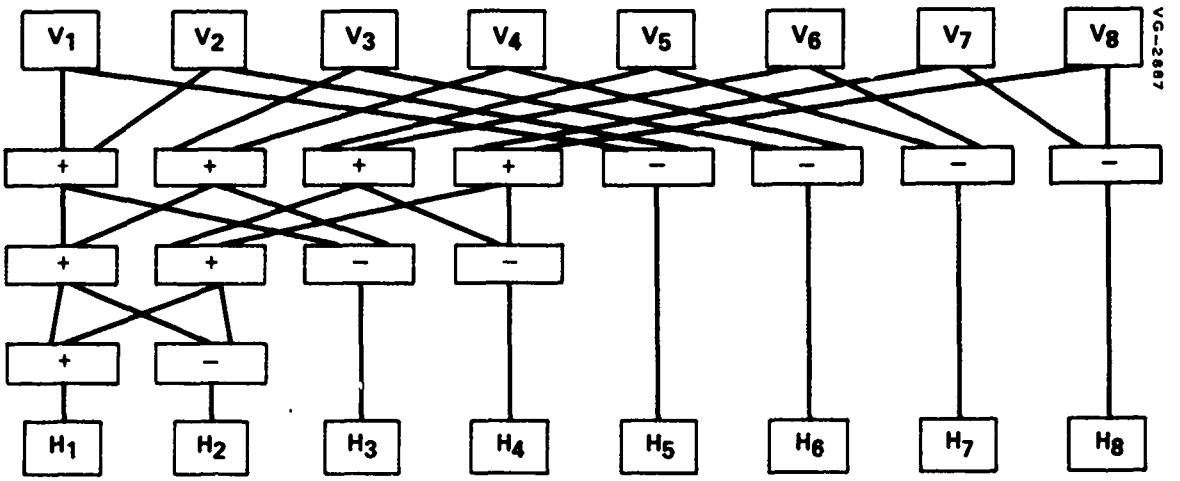

TRANSFORMED VECTOR $HV = (H_1, H_2, H_3, H_4, H_5, H_6, H_7, H_8)$

Figure 3-24. Rationalized Haar fast algorithm.

Derivation of Rational Haar Transform

The following illustrates by example the derivation of the rational Haar transform matrix. The case $N = 2^3 = 8$ is sufficiently complex to form a good example. The Haar transform matrix H is

$$H = \frac{1}{2\sqrt{2}} \begin{bmatrix} 1 & 1 & 1 & 1 & 1 & 1 & 1 & 1 \\ 1 & 1 & 1 & 1 & -1 & -1 & -1 & -1 \\ \sqrt{2} & \sqrt{2} & -\sqrt{2} & -\sqrt{2} & 0 & 0 & 0 & 0 \\ 0 & 0 & 0 & 0 & \sqrt{2} & \sqrt{2} & -\sqrt{2} & -\sqrt{2} \\ 2 & -2 & 0 & 0 & 0 & 0 & 0 & 0 \\ 0 & 0 & 2 & -2 & 0 & 0 & 0 & 0 \\ 0 & 0 & 0 & 0 & 2 & -2 & 0 & 0 \\ 0 & 0 & 0 & 0 & 0 & 0 & 2 & -2 \end{bmatrix}$$

, which can be

factored as $H = F\hat{H}$ where

$$F = \frac{1}{2\sqrt{2}} \begin{bmatrix} 1 & 0 & 0 & 0 & 0 & 0 & 0 & 0 \\ 0 & 1 & 0 & 0 & 0 & 0 & 0 & 0 \\ 0 & 0 & \sqrt{2} & 0 & 0 & 0 & 0 & 0 \\ 0 & 0 & 0 & \sqrt{2} & 0 & 0 & 0 & 0 \\ 0 & 0 & 0 & 0 & 2 & 0 & 0 & 0 \\ 0 & 0 & 0 & 0 & 0 & 2 & 0 & 0 \\ 0 & 0 & 0 & 0 & 0 & 0 & 2 & 0 \\ 0 & 0 & 0 & 0 & 0 & 0 & 0 & 2 \end{bmatrix}$$

and

$$\hat{H} = \begin{bmatrix} 1 & 1 & 1 & 1 & 1 & 1 & 1 & 1 \\ 1 & 1 & 1 & 1 & -1 & -1 & -1 & -1 \\ 1 & 1 & -1 & -1 & 0 & 0 & 0 & 0 \\ 0 & 0 & 0 & 0 & 1 & 1 & -1 & -1 \\ 1 & -1 & 0 & 0 & 0 & 0 & 0 & 0 \\ 0 & 0 & 1 & -1 & 0 & 0 & 0 & 0 \\ 0 & 0 & 0 & 0 & 1 & -1 & 0 & 0 \\ 0 & 0 & 0 & 0 & 0 & 0 & 1 & -1 \end{bmatrix}$$

where $\hat{H}$ is the rationalized Haar matrix. $\hat{H}$ itself can be further factored into a product of three matrices: $\hat{H}_1$, $\hat{H}_2$, and $\hat{H}_3$.

$$\hat{H} = \hat{H}_3 \hat{H}_2 \hat{H}_1 =$$

$$= \begin{bmatrix} 1 & 1 & 0 & 0 & 0 & 0 & 0 & 0 \\ 1 & -1 & 0 & 0 & 0 & 0 & 0 & 0 \\ 0 & 0 & 1 & 0 & 0 & 0 & 0 & 0 \\ 0 & 0 & 0 & 1 & 0 & 0 & 0 & 0 \\ 0 & 0 & 0 & 0 & 1 & 0 & 0 & 0 \\ 0 & 0 & 0 & 0 & 0 & 1 & 0 & 0 \\ 0 & 0 & 0 & 0 & 0 & 0 & 1 & 0 \\ 0 & 0 & 0 & 0 & 0 & 0 & 0 & 1 \end{bmatrix} \cdot \begin{bmatrix} 1 & 1 & 0 & 0 & 0 & 0 & 0 & 0 \\ 0 & 0 & 1 & 1 & 0 & 0 & 0 & 0 \\ 1 & -1 & 0 & 0 & 0 & 0 & 0 & 0 \\ 0 & 0 & 1 & -1 & 0 & 0 & 0 & 0 \\ 0 & 0 & 0 & 0 & 1 & 0 & 0 & 0 \\ 0 & 0 & 0 & 0 & 0 & 1 & 0 & 0 \\ 0 & 0 & 0 & 0 & 0 & 0 & 1 & 0 \\ 0 & 0 & 0 & 0 & 0 & 0 & 0 & 1 \end{bmatrix} \cdot \begin{bmatrix} 1 & 1 & 0 & 0 & 0 & 0 & 0 & 0 \\ 0 & 0 & 1 & 1 & 0 & 0 & 0 & 0 \\ 0 & 0 & 0 & 0 & 1 & 1 & 0 & 0 \\ 0 & 0 & 0 & 0 & 0 & 0 & 1 & 1 \\ 1 & -1 & 0 & 0 & 0 & 0 & 0 & 0 \\ 0 & 0 & 1 & -1 & 0 & 0 & 0 & 0 \\ 0 & 0 & 0 & 0 & 1 & -1 & 0 & 0 \\ 0 & 0 & 0 & 0 & 0 & 0 & 1 & -1 \end{bmatrix}$$

Hence, $H = F\hat{H}_3 \hat{H}_2 \hat{H}_1$

The fact that H can be factored into three simpler matrices gives rise to a fast algorithm for computing the rational Haar transform of a vector V. This algorithm is depicted in Figure 3-24. Note that each computational level in the algorithm represents one matrix multiply. To take the Haar

transform of a vector V, the fast algorithm is first applied to the vector and then each resultant term is weighted according to the matrix F. The inverse Haar transform algorithm is similar. For a combination of forward and inverse Haar transforms, the weighting terms reduce to powers of 2, or binary shifts.

The forward and inverse Haar transform of Image I is

$$H^T H(I) = (F\hat{H})^T F\hat{H}I$$

$$= \hat{H}^T F^T F\hat{H}I$$

$$= \hat{H}^T FF\hat{H}I$$

$$= \hat{H}^T F^2 \hat{H}I$$

where

$$F^2 = 1/8 \begin{bmatrix} 1 & 0 & 0 & 0 & 0 & 0 & 0 & 0 \\ 0 & 1 & 0 & 0 & 0 & 0 & 0 & 0 \\ 0 & 0 & 2 & 0 & 0 & 0 & 0 & 0 \\ 0 & 0 & 0 & 2 & 0 & 0 & 0 & 0 \\ 0 & 0 & 0 & 0 & 4 & 0 & 0 & 0 \\ 0 & 0 & 0 & 0 & 0 & 4 & 0 & 0 \\ 0 & 0 & 0 & 0 & 0 & 0 & 4 & 0 \\ 0 & 0 & 0 & 0 & 0 & 0 & 0 & 4 \end{bmatrix}$$

The transpose of H, H^T, is employed in the above equation as the inverse Haar transform since H is real and orthogonal, i.e., $H^{-1} = H^T$. In the following equations H^{-1} will be used ir place of H^T.

Haar Transform Crispening

High spatial frequencies of an image that have been attenuated can be restored via transform filtering. This is normally called "image restoration." "Image enhancement" results when further emphasis or amplification is placed or selected spatial frequencies of the image. Early attempts at image "crispening" or "edge enhancement" were implemented by using differential operators in the spatial domain. A generalized set of even order

partial derivatives with constant coefficients can be used to form the crispening function as follows:

$$\hat{p}(x, y) = A\, p(x, y) + B\, \nabla^2 p(x, y) + C\, \nabla^4 p(x, y) + \ldots$$

where:

$p(x, y)$ = a picture element at location x, y

$\hat{p}(x, y)$ = enhanced picture element at x, y

$\nabla^n = n^{th}$ gradient operator

$$= \left(\frac{\delta^n}{\delta x^n} + \frac{\delta^n}{\delta y^n} \right)$$

A, B, C, ... = arbitrary constants

The simplest crispening operator is given by

$$\hat{p}(x, y) = p(x, y) - k\, \nabla^2 p(x, y) \qquad (1)$$

where k is a constant.

The second partial derivative is involved in the crispening operator since it defines the arcs or brightness curvatures in the original image. For example, consider the one-dimensional function p (x) shown in Figure 3-25a. For one-dimensional crispening the n^{th} gradient operator can be replaced with the n^{th} partial derivative with respect to the appropriate dimension $\left(\text{either} \frac{\delta^n}{\delta x^n} \text{ or } \frac{\delta^n}{\delta y^n} \right)$. The second partial derivative with respect to x is plotted in Figure 3-25b. Figure 3-25c demonstrates the results of applying Equation (1) to the function p (x), namely, that the function has been enhanced by "sharpening" up or "crispening" the edges.

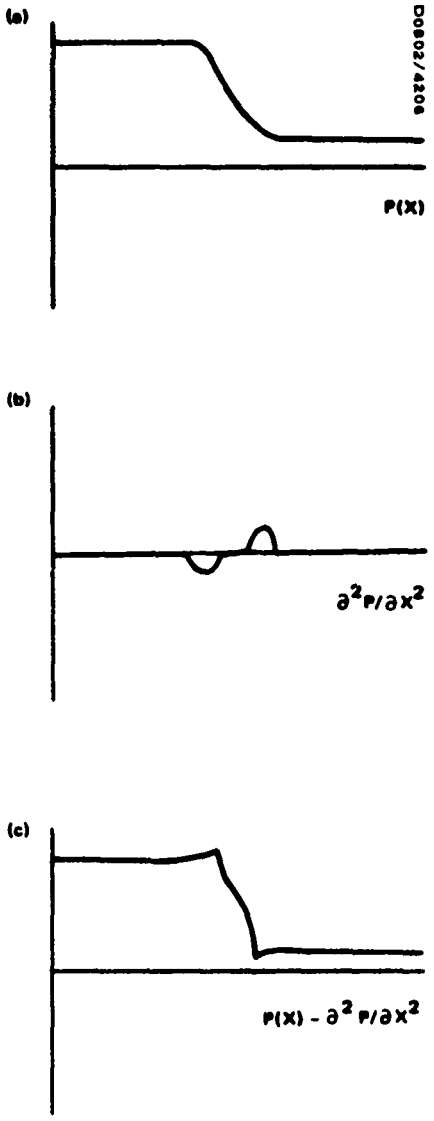

Figure 3-25. Geometric significance of 2nd partial derivative.

As mentioned before, the operator $1 - kD_x^2$ when applied to a function p(x) acts as a crispening operator, where $D_x^2 = \frac{\delta^2}{\delta x^2}$. We have chosen to implement this one-dimensional crispening operator in the Haar domain for image enhancement. The reason for this is that most resolution loss from a sensor system is one-dimensional in nature. In a TV system, for example, horizontal resolution requires the greatest system bandwidth. All the Haar transform crispening done for this study has been done in the horizontal dimension.

The following describes in detail the derivation of the one-dimensional crispening function, G, that when applied in the Haar domain, achieves the equivalent of the crispening operator. Let the following variables hold for this derivation:

H = Haar transform

H^{-1} = inverse Haar transform

$\hat{H}$ = rationalized Haar transform

$\hat{H}^{-1}$ = inverse rationalized Haar transform

I = image

G = Haar domain crispening operator

$\hat{I}$ = enhanced image

As shown previously $H = F\hat{H}$ and $H^{-1} = \hat{H}^{-1}F$.
Now the spatial domain crispening operator is

$$\hat{I} = \left(I - kD_x^2\right) I.$$

However, we wish to achieve similar crispening in the Haar domain such that

$$\hat{I} = H^{-1}\left[G(HI)\right] = \left(1 - kD_x^2\right) I. \qquad (2)$$

From this equation we can derive the operator G such that when the product of G and the Haar transform of an image is inverse Haar transformed, the equivalent of the spatial domain crispening operator $(1 - kD_x^2)$ results.
From (2),

$$H^{-1}GHI = (1 - kD_x^2)\, I$$

and

$$H^{-1}GH = 1 - kD_x^2$$

then solving for G

$$GH = H - H\,kD_x^2$$

$$G = HH^{-1} - HkD_x^2 H^{-1}$$

$$= 1 - kHD_x^2 H^{-1}$$

Since $H = F\hat{H}$, then substituting

$$G = 1 - kF\hat{H}D_x^2 (F\hat{H})^{-1}$$

$$= 1 - kF\hat{H}D_x^2\hat{H}^{-1}F \qquad (3)$$

Therefore when G is applied to the Haar transform of an image via (2), crispening results.

Implementation of the Haar Crispening Operator

The Haar transform domain crispening operator G was previously derived such that an image I is enhanced by the following equation:

$$\hat{I} = H^{-1}GHI \qquad (4)$$

where $G = 1 - kF\hat{H}D_x^2\hat{H}^{-1}F$.

Now by substitution

$$\hat{I} = H^{-1}(1 - kF\hat{H}D_x^2\hat{H}^{-1}F)\,HI.$$

Reducing the Haar transform to rational transforms where $H = F\hat{H}$, yields

$$\hat{I} = (F\hat{H})^{-1}(1 - kF\hat{H}D_x^2\hat{H}^{-1}F)\,F\hat{H}I$$

$$= (1 - k\hat{H}^{-1}F^2\hat{H}D_x^2\hat{H}^{-1}F^2\hat{H})\,I \qquad (5)$$

Letting

$$A = F^2 \hat{H} D_x^2 \hat{H}^{-1} F^2 \tag{6}$$

we have from (5)

$$\hat{I} = (1 - k\hat{H}^{-1} A \hat{H}) I \tag{7}$$

where A now represents the Haar transform domain weighting function that when applied to the rationalized Haar transform of an image produces crispening. Note that (6) contains F^2 matrices that are conveniently powers of two, simplifying hardware mechanization.

Since the forward and inverse rational Haar transforms are easy to compute, the complexity of the entire crispening process of equation (7) relies upon the complexity of the matrix A. Note that the matrix A is independent of the input image and can, therefore, be computed before the processing occurs.

Consider the case where the size of the input image is 8 x 8. Making use of the 2^{nd} order finite difference operator, D_x^2 can be written in the following matrix form:

$$D_x^2 = \begin{bmatrix} 1 & -2 & 1 & 0 & 0 & 0 & 0 & 0 \\ 1 & -2 & 1 & 0 & 0 & 0 & 0 & 0 \\ 0 & 1 & -2 & 1 & 0 & 0 & 0 & 0 \\ 0 & 0 & 1 & -2 & 1 & 0 & 0 & 0 \\ 0 & 0 & 0 & 1 & -2 & 1 & 0 & 0 \\ 0 & 0 & 0 & 0 & 1 & -2 & 1 & 0 \\ 0 & 0 & 0 & 0 & 0 & 1 & -2 & 1 \\ 0 & 0 & 0 & 0 & 0 & 1 & -2 & 1 \end{bmatrix}$$

From above we know that

$$F^2 = 1/8 \begin{bmatrix} 1 & 0 & 0 & 0 & 0 & 0 & 0 & 0 \\ 0 & 1 & 0 & 0 & 0 & 0 & 0 & 0 \\ 0 & 0 & 2 & 0 & 0 & 0 & 0 & 0 \\ 0 & 0 & 0 & 2 & 0 & 0 & 0 & 0 \\ 0 & 0 & 0 & 0 & 4 & 0 & 0 & 0 \\ 0 & 0 & 0 & 0 & 0 & 4 & 0 & 0 \\ 0 & 0 & 0 & 0 & 0 & 0 & 4 & 0 \\ 0 & 0 & 0 & 0 & 0 & 0 & 0 & 4 \end{bmatrix} \quad \text{and} \quad \hat{H} = \begin{bmatrix} 1 & 1 & 1 & 1 & 1 & 1 & 1 & 1 \\ 1 & 1 & 1 & 1 & -1 & -1 & -1 & -1 \\ 1 & 1 & -1 & -1 & 0 & 0 & 0 & 0 \\ 0 & 0 & 0 & 0 & 1 & 1 & -1 & -1 \\ 1 & -1 & 0 & 0 & 0 & 0 & 0 & 0 \\ 0 & 0 & 1 & -1 & 0 & 0 & 0 & 0 \\ 0 & 0 & 0 & 0 & 1 & -1 & 0 & 0 \\ 0 & 0 & 0 & 0 & 0 & 0 & 1 & -1 \end{bmatrix}$$

Therefore,

$$A = F^{2}\hat{H}D_{x}{}^{2}\hat{H}^{-1}F^{2} = 4 \begin{bmatrix} 0 & 0 & -1 & 1 & 5 & 1 & -1 & -5 \\ 0 & -1 & 0 & 0 & 5 & 3 & 3 & 5 \\ 0 & 1 & -7 & -1 & 14 & 4 & -2 & 0 \\ 0 & 1 & -1 & -7 & 0 & -2 & 4 & 14 \\ 0 & 0 & 0 & 0 & 0 & 0 & 0 & 0 \\ 0 & 2 & 2 & -2 & -4 & -24 & -4 & 0 \\ 0 & 2 & -2 & 2 & 0 & -4 & -24 & -4 \\ 0 & 0 & 0 & 0 & 0 & 0 & 0 & 0 \end{bmatrix}$$

In practice, the implementation of the matrix A is prohibitive due to all of its non-zero terms. Therefore, two engineering approximations can be taken to reduce the matrix A to one that can be easily implemented in hardware. They ar to set all off-diagonal entries in A to zero and to set all diagonal entries in A to the nearest power of two. Mathematically, the two steps tend to offset each other and, therefore, cause this to be a good approximation to the actual A matrix.

Therefore, the matrix A approximation is

$$A = 4 \begin{bmatrix} 0 & 0 & 0 & 0 & 0 & 0 & 0 & 0 \\ 0 & -1 & 0 & 0 & 0 & 0 & 0 & 0 \\ 0 & 0 & -8 & 0 & 0 & 0 & 0 & 0 \\ 0 & 0 & 0 & -8 & 0 & 0 & 0 & 0 \\ 0 & 0 & 0 & 0 & -32 & 0 & 0 & 0 \\ 0 & 0 & 0 & 0 & 0 & -32 & 0 & 0 \\ 0 & 0 & 0 & 0 & 0 & 0 & -32 & 0 \\ 0 & 0 & 0 & 0 & 0 & 0 & 0 & -32 \end{bmatrix}$$

The crispening process using the Haar transform can now be totally implemented by using only addition, subtraction and binary shifts. Figure 3-26 summarizes the Haar transform crispening technique.

Now that the derivation of the crispening operator is complete only one variable remains to be determined; the value of k from equation (7). Note that k determines the amount of crispening to be added to the original image. Figure 3-27 shows the effect of varying levels of k where the crispening is applied only to the horizontal dimension. Inspection of the results of Figure 3-27 shows that k = 1 provides a good amount of crispening for most cases.

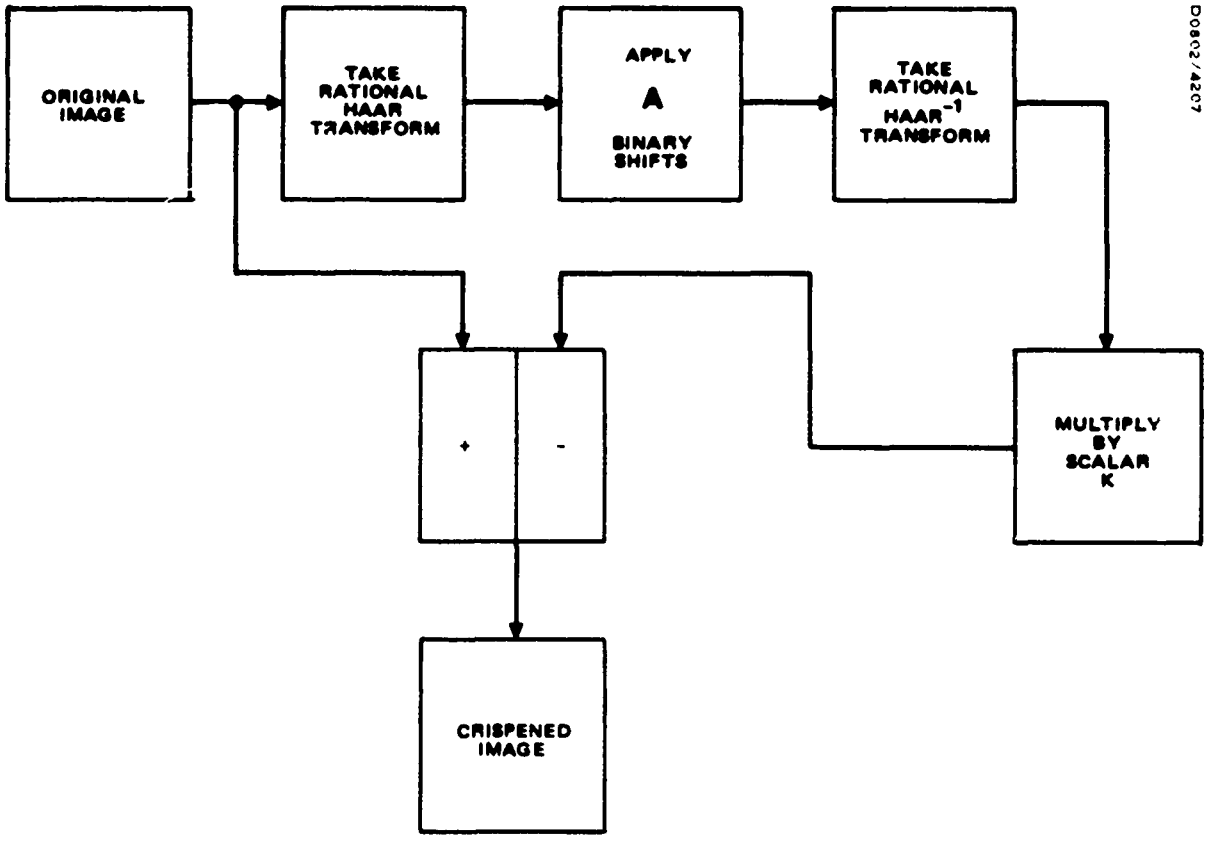

Figure 3-26. Block diagram of crispening operator.

a) Original

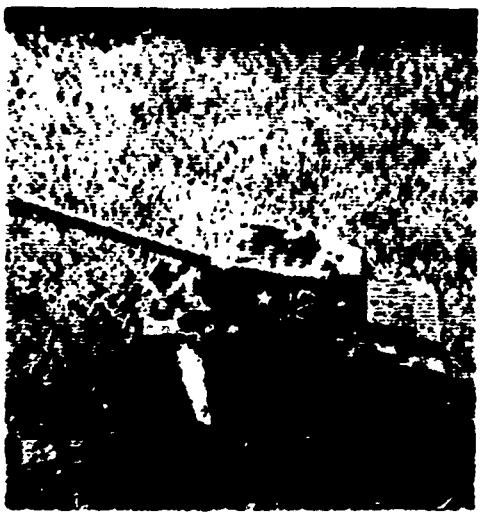

b) k = 1

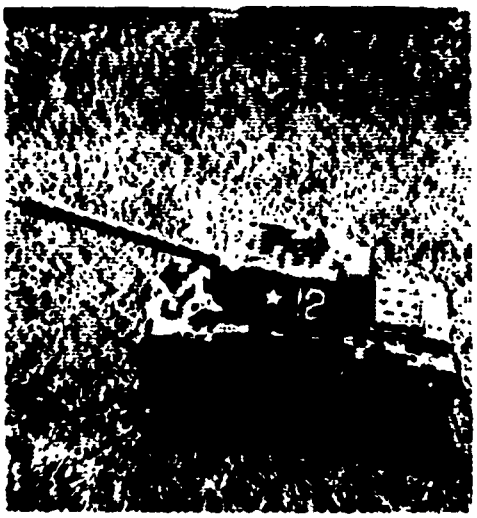

c) k = 2

d) k = 3

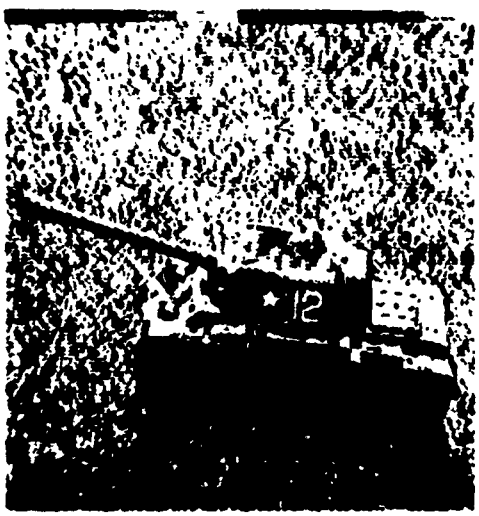

e) k = 4

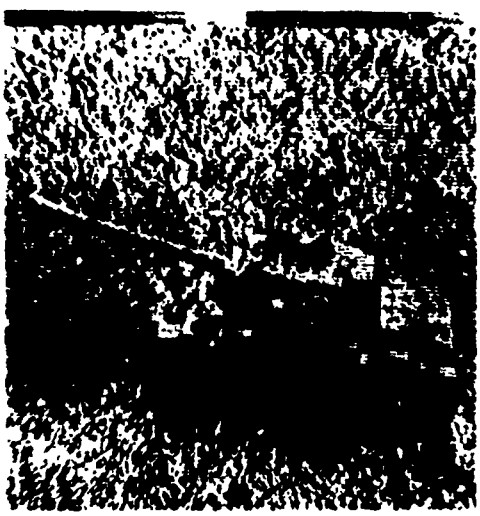

f) k = 5

Figure 3-27. Varying levels of Haar transform crispening due to value of k from equation (7).

4.0 EVALUATION OF ENHANCEMENT TECHNIQUES

This section describes the results of two evaluations of the enhancement techniques (LAHE, LABGC, HTC):

- Human Factors Evaluation
- Hardware Implementation Evaluation

The human factors evaluation analyzed subjectively the utility and viewer acceptance of each enhancement technique. This was done by first enhancing an ensemble of eleven images representative of 3 different sensor systems. The best of each technique was used. Then, ten subjects evaluated these enhancements using the original image as a reference.

The hardware implementation evaluation was performed by making a functional block diagram of each technique. Based on these, an estimate was made of the number of integrated circuits required for each.

The results of these evaluations are described in the following sections.

4.1 IMAGE ENHANCEMENT EVALUATION

Summary

The image enhancement evaluation was conducted to obtain data on viewer acceptance and utility of enhanced images. Ten subjects with extensive backgrounds in the development, display, and interpretation of sensor imagery, subjectively evaluated eleven tactical scenes Figures 4-1a through 4-11a in terms of seven typical operational tasks. The evaluation was made on a seven point scale, with the original unenhanced image presentation serving as the base unit (4) and the enhanced images being judged as better (5, 6, or 7) or worse (3, 2, or 1) than the original image.

The resulting data support the following conclusions:

1. Viewer acceptance and utility of enhanced imagery is dependent upon the sensor being used, the scene, and the operator task.
2. Enhanced imagery is most useful in detailed interpretation tasks conducted at short to medium range using optical sensors.
3. Enhancement techniques are of unknown value when applied to synthetic aperture radar imagery.

In summary, this brief evaluation strongly indicates that image enhancement techniques can be utilized to improve viewer interpretation performance of critical tactical tasks which involve overall target area orientation, target detection, identification and designation.

Evaluation Task

The evaluation task reflected the following factors:

1. Sensors – Samples of TV, FLIR, and synthetic aperture radar imagery were used.
2. Target scenes – A series of 11 target scenes were chosen as being representative of a range of operational tactical target scenes.
3. Image enhancement techniques – Each target scene was presented in a set of four photographs as follows:
   - Original unenhanced sensor image, Figures 4-1a through 4-11a.
   - A Local Area Histogram Equalized, 4 x 4 center box image. Figures 4-1b through 4-11b.
   - A Local Area Brightness and Gain Control statistical gain 16/4 image. Figures 4-1c through 4-11c.
   - A Haar Transform Crispened image with k = 1. Figures 4-1d through 4-11d.
4. Subjects – 10 subjects evaluated the imagery. Five subjects were human factors personnel, five were display systems engineers. All subjects were experienced in the interpretation of one or more types of sensor imagery.
5. Operational tasks – The imagery was evaluated relative to its potential use in the following set of operational tasks:
   - Vehicle control
   - Sensor control

a) Original.

b) Local Area Histogram Equalized, 4 x 4 center box.

c) Local Area Brightness and Gain Control, statistical gain 16/4.

d) Haar Transform Crispened, k = 1.

Figure 4-1. TV imagery – tank (close-in).

a) Original.

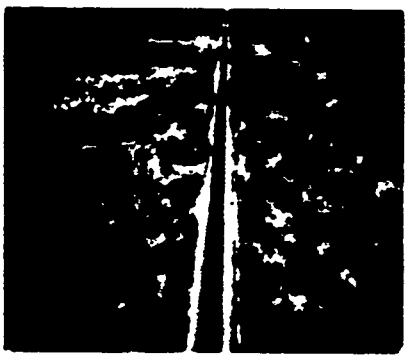

b) Local Area Histogram Equalized, 4 x 4 center box.

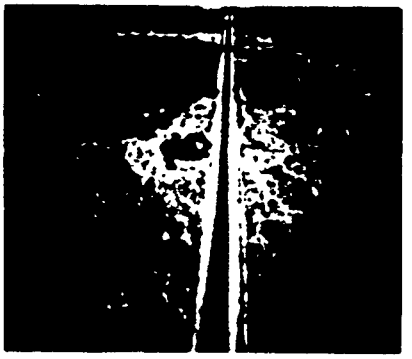

c) Local Area Brightness and Gain Control, statistical gain 16/4.

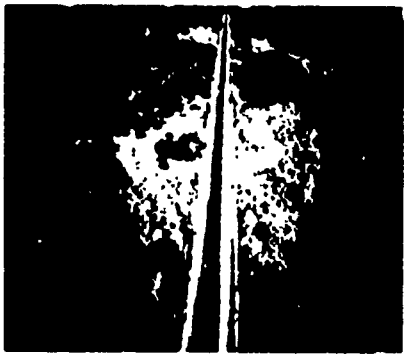

d) Haar Transform Crispened, k = 1.

Figure 4-2. TV imagery – road (medium range).

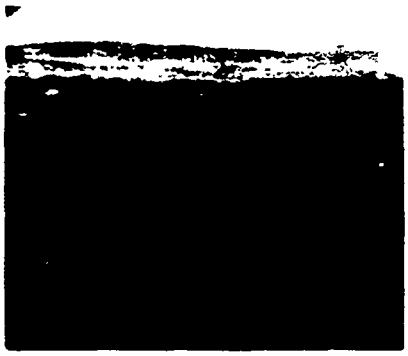

a) Original.

b) Local Area Histogram Equalizer, 4 x 4 center box.

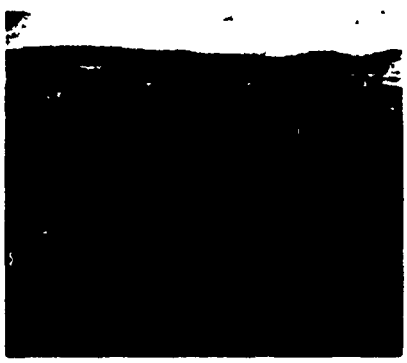

c) Local Area Brightness and Gain Control, statistical gain 16/4.

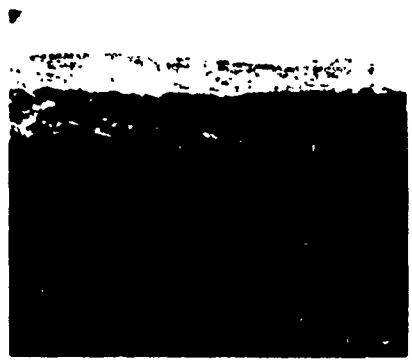

d) Haar Transform Crispened, k = 1.

Figure 4-3. TV imagery – terrain (long range).

a) Original.

b) Local Area Histogram Equalized, 4 x 4 center box.

c) Local Area Brightness and Gain Control, statistical gain 16/4.

d) Haar Transform Crispened, k = 1.

Figure 4-4. FLIR imagery – ship (close-in).

a) Original.

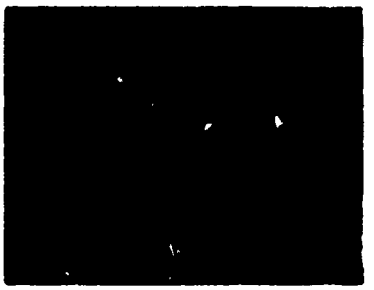

b) Local Area Histogram Equalized, 4 x 4 center box.

c) Local Area Brightness and Gain Control, statistical gain 16/4.

d) Haar Transform Crispened, k = 1.

Figure 4-5. FLIR imagery – tank (close-in).

a) Original.

b) Local Area Histogram Equalized, 4 x 4 center box.

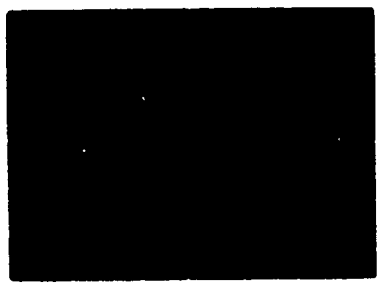

c) Local Area Brightness and Gain Control, statistical gain 16/4.

d) Haar Transform Crispened, k = 1.

Figure 4-6. FLIR imagery – power plant (short range).

a) Original.

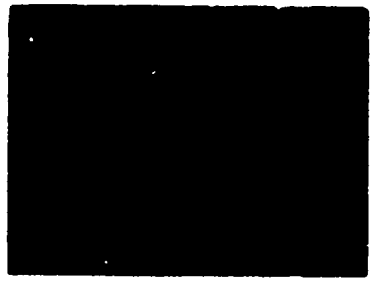

b) Local Area Histogram Equalized, 4 x 4 center box.

c) Local Area Brightness and Gain Control, statistical gain 16/4.

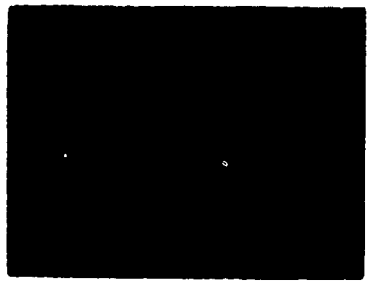

d) Haar Transform Crispened, k = 1.

Figure 4-7. FLIR imagery – tank (short range).

a) Original.

b) Local Area Histogram Equalized, 4 x 4 center box.

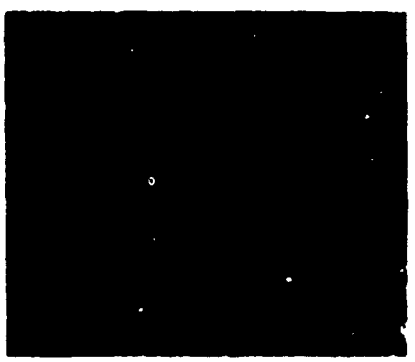

c) Local Area Brightness and Gain Control, statistical gain 16/4.

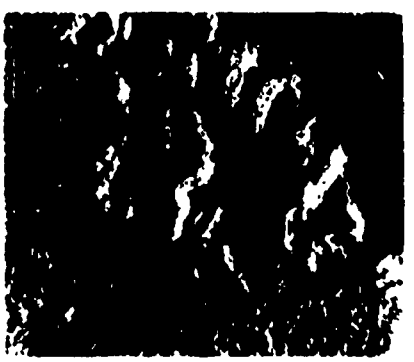

d) Haar Transform Crispened, k - 1.

Figure 4-8. Radar imagery – mountains.

a) Original.

b) Local Area Histogram Equalized, 4 x 4 center box.

c) Local Area Brightness and Gain Control, statistical gain 16/4.

d) Haar Transform Crispened, k = 1.

Figure 4-9. Radar imagery – road.

a) Original.

b) Local Area Histogram Equalized, 4 x 4 center box.

c) Local Area Brightness and Gain Control, statistical gain 16/4.

d) Haar Transform Crispened, k = 1.

Figure 4-10. Radar imagery – fields.

a) Original.

b) Local Area Histogram Equalized, 4 x 4 center box.

c) Local Area Brightness and Gain Control, statistical gain 16/4.

d) Haar Transform Crispened, k = 1.

Figure 4-11. Radar imagery – river.

- Orientation
- Target detection
- Target recognition
- Target identification
- Target designation

6. Evaluation rating scale – The imagery was evaluated using the following scale:

   7 Excellent
   6 Very good
   5 Good
   4 Acceptable
   3 Fair
   2 Poor
   1 Not usable

The original sensor image was defined as acceptable (4) for all scenes. The enhanced images were rated relative to the original.

Results

Each subject evaluated the eleven tactical scenes relative to the specific operational tasks pertinent to the scene. The average rating scores for the three enhancement techniques are presented in Tables 4-1 (LAHE), 4-2 (LABGC), and 4-3 (HTC). Comparative data for the three sensors are depicted in Figures 4-12 (TV), 4-13 (FLIR), and 4-14 (radar).

Viewer rating scores were strongly influenced by sensor, scene, and task factors in addition to the enhancement technique being used. The impact of these factors is reflected in the following data summaries.

- Sensor - The average ratings by sensor are as follows:

	TV	FLIR	RADAR
LAHE	4.6	4.35	4.0
LABGC	4.9	4.4	3.7
HTC	4.2	3.8	3.55
AVE	4.57	4.20	3.75

TABLE 4-1. AVERAGE RATINGS – LAHE ENHANCEMENT

	TV			FLIR				RADAR				
Operator Task \ Scene	1	2	3	4	5	6	7	8	9	10	11	Task Ave
Vehicle Control	X	5.3	2.9	X	X	X	X	3.9	4.0	4.0	4.1	4.2
Sensor Control	4.2	5.2	3.5	4.2	4.4	4.1	4.0	3.9	4.1	3.8	4.2	4.2
Orientation	X	5.3	3.6	X	X	4.2	X	3.7	4.0	3.9	4.5	4.1
Target Detection	X	5.4	3.8	X	X	4.3	X	3.6	4.3	3.2	4.4	4.1
Target Recognition	X	5.5	X	X	X	4.2	X	3.9	4.3	X	4.2	4.4
Target Identification	5.7	5.5	X	4.6	4.6	4.2	4.2	X	X	X	4.3	4.7
Target Designation	4.8	5.5	X	4.7	4.5	4.4	4.5	4.1	4.3	X	4.4	4.6
Average	4.9	5.4	3.5	4.5	4.5	4.2	4.2	3.8	4.2	3.7	4.3	4.3
	4.6			4.35				4.0				

– Average for all evaluations

TABLE 4-2. AVERAGE RATINGS – LABGC ENHANCEMENT

Operator Task \ Scene	TV			FLIR				RADAR				
	1	2	3	4	5	6	7	8	9	10	11	Task Ave
Vehicle Control	X	5.1	4.6	X	X	X	X	3.5	3.9	3.5	3.7	4.1
Sensor Control	4.3	5.1	4.7	4.0	4.8	3.9	4.1	3.5	4.2	3.4	3.7	4.2
Orientation	X	5.2	4.8	X	X	4.2	X	3.5	4.1	3.4	3.7	4.1
Target Detection	X	5.1	4.6	X	X	4.3	X	3.3	4.6	3.3	4.0	4.2
Target Recognition	X	4.9	X	X	X	4.2	X	3.3	4.3	X	4.1	4.1
Target Identification	5.3	5.1	X	4.2	5.3	4.1	4.5	X	X	X	4.0	4.6
Target Designation	4.7	4.9	X	4.2	4.8	4.1	4.2	3.4	4.5	X	4.0	4.3
Average	4.8	5.1	4.8	4.1	5.0	4.1	4.3	3.4	4.3	3.4	3.8	4.4
	4.9			4.4				3.7				

4.4 – Average for all evaluations

TABLE 4-3. AVERAGE RATINGS – HTC ENHANCEMENT

Operator Task	Scene	IV 1	IV 2	IV 3	FLIR 4	FLIR 5	FLIR 6	FLIR 7	RADAR 8	RADAR 9	RADAR 10	RADAR 11	Task Ave
Vehicle Control		X	4.4	3.9	X	X	X	X	3.6	3.8	3.8	3.9	3.9
Sensor Control		4.3	4.1	4.1	4.3	4.0	3.2	3.8	3.4	3.5	3.4	3.7	3.8
Orientation		X	4.4	4.0	X	X	3.2	X	3.5	3.8	3.4	3.8	3.7
Target Detection		X	4.2	4.1	X	X	3.3	X	3.4	3.5	2.9	3.8	3.6
Target Recognition		X	3.6	X	X	X	3.2	X	3.6	3.6	X	3.6	3.6
Target Identification		4.8	3.8	X	4.1	3.8	3.1	3.5	X	X	X	3.5	3.8
Target Designation		4.5	4.1	X	4.1	4.1	3.6	3.7	3.3	3.6	X	3.8	3.9
	Average	4.5	4.1	4.0	4.2	4.0	3.3	3.7	3.5	3.6	3.4	3.7	3.85
			4.2			3.8				3.55			

3.85 – Average for all evaluations

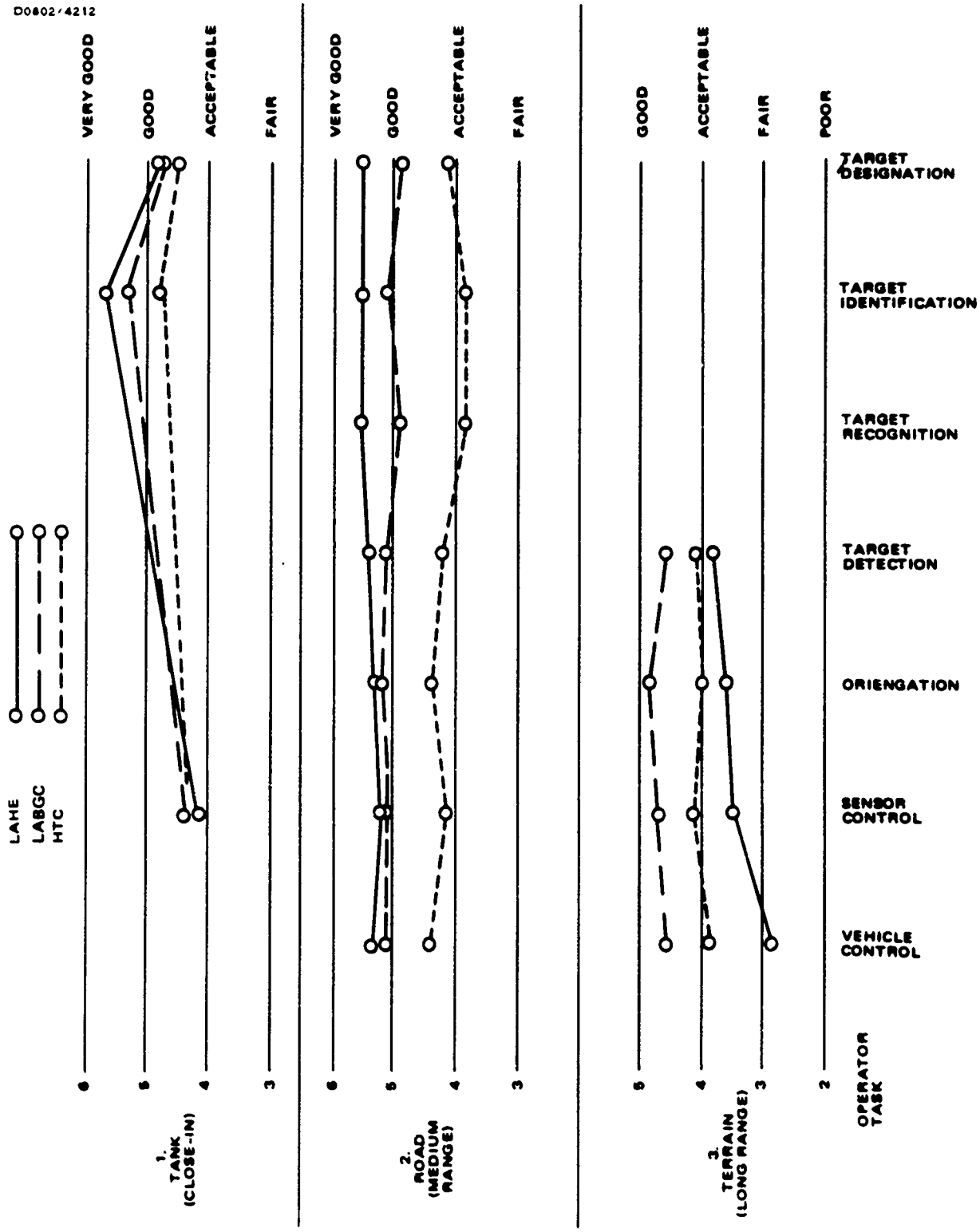

Figure 4-12. Average ratings — TV.

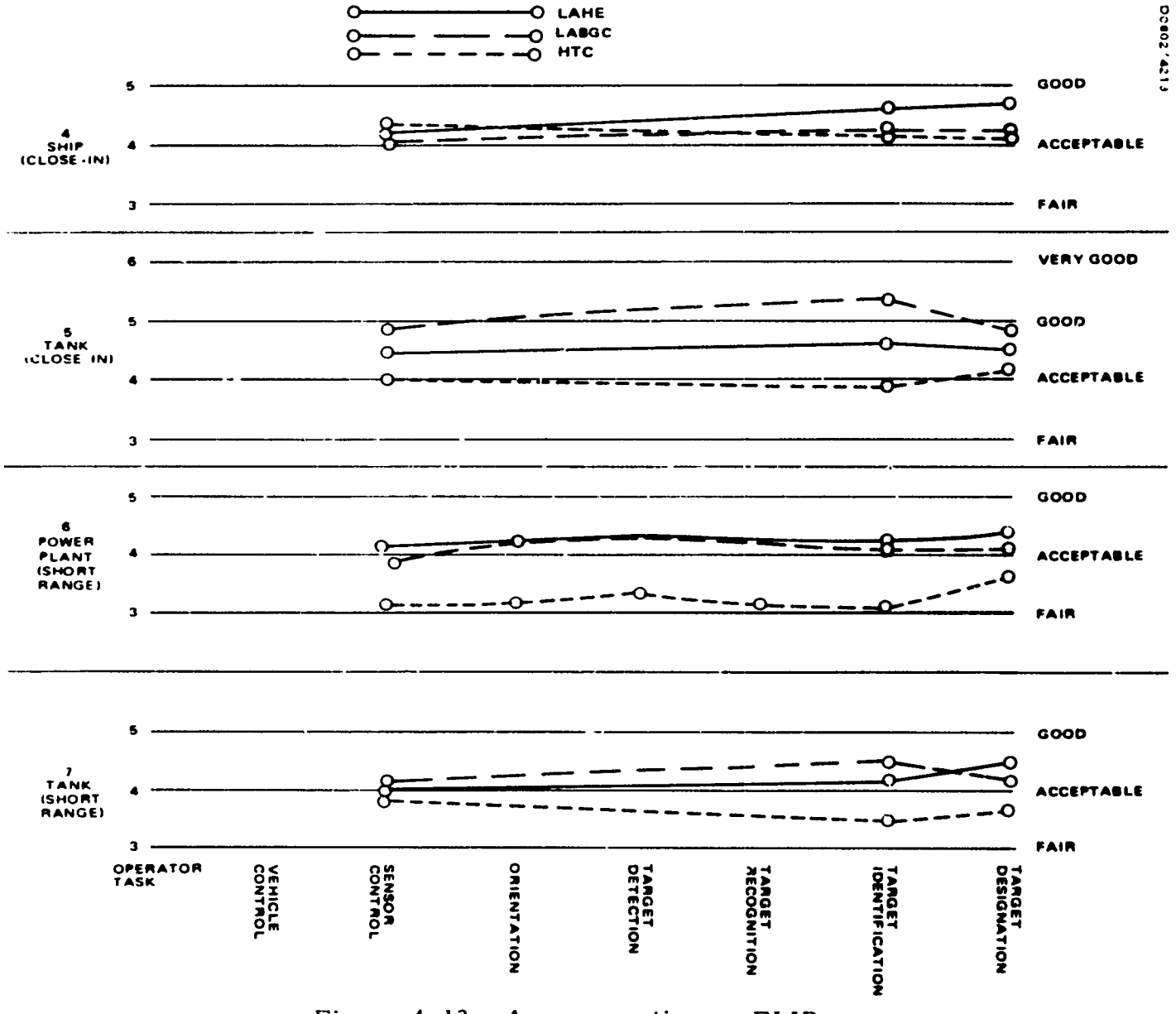

Figure 4-13. Average ratings – FLIR.

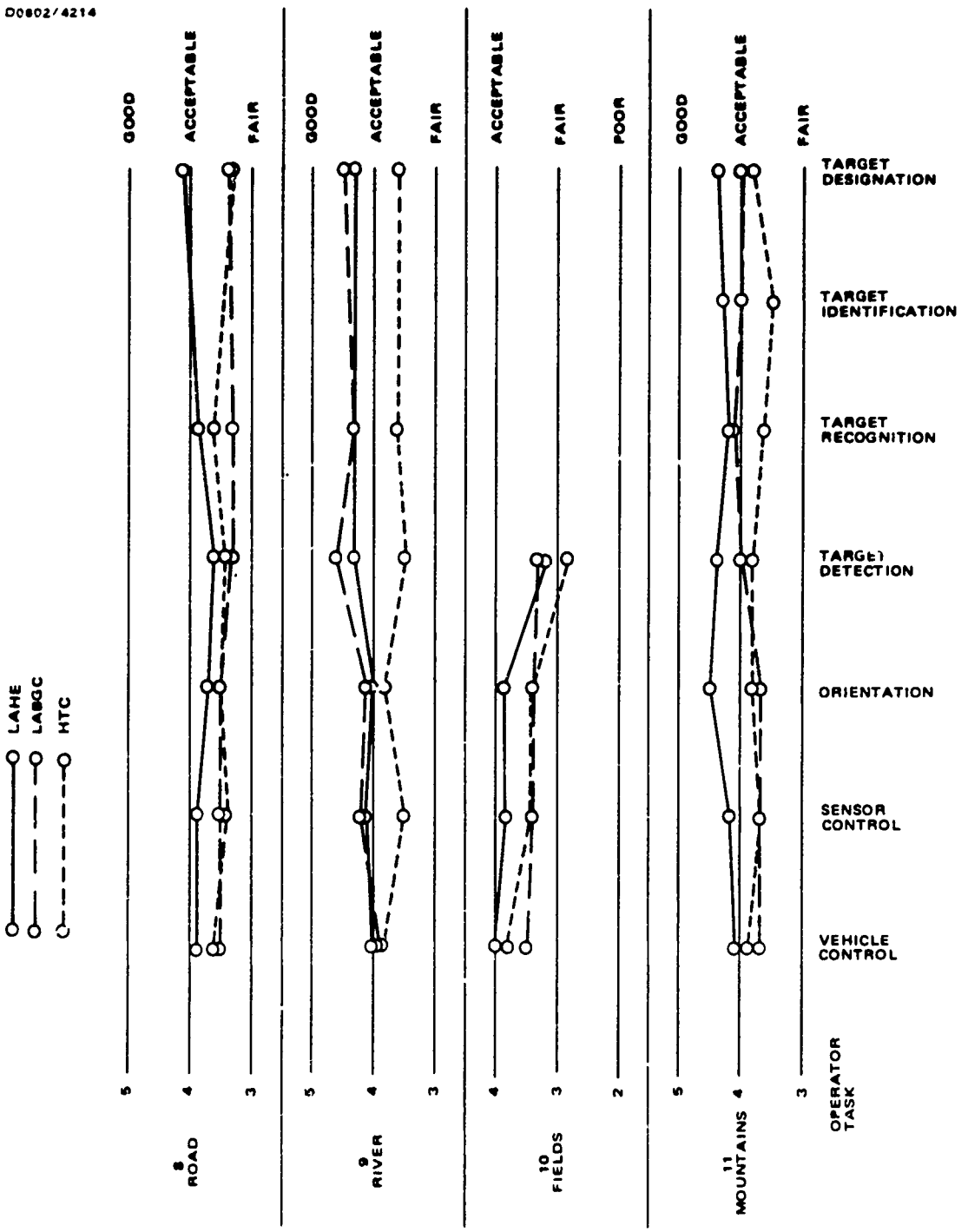

Figure 4-14. Average ratings — RADAR.

For each enhancement technique, the TV images were evaluated as being most improved over the original. FLIR images were judged as better with LAHE and LABGC enhancement, but less acceptable with HTC enhancement. Enhancement had virtually no effect on radar images (LAHE and LABGC) except for the HTC technique which reduced image acceptability.

- Scene - Ratings varied widely for the different scenes. The three highest rated scenes by enhancement technique were as follows:

LAHE	2(5.4)	1(4.9)	4 & 5 (4.5)
LABGC	2(5.1)	5(5.0)	1 & 3 (4.8)
HTC	1(4.5)	4(4.2)	2 (4.1)

In general, close-in and medium range images (1, 2, 4, and 5) benefitted most from enhancement.

- Operator task - In specific cases such as target identification (TV) high ratings were achieved for all enhancement techniques. Highest overall averages for individual tasks were recorded for the target identification and target designation tasks. As shown by the task averages (Tables 4-1, 4-2, and 4-3), the highest ratings were as follows:

LAHE	TGT ID	TGT DESIG
	4.7	4.6
LABGC	TGT ID	TGT DESIG
	4.6	4.3
HTC	TGT DESIG and VEH CONT	TGT ID
	3.9	3.8

These data indicate that operator tasks requiring use of high image detail benefit most from image enhancement.

- Enhancement technique - In summary, the data from this evaluation indicate that for detailed interpretation tasks, using optical sensors at short and medium ranges, image enhancement improves the viewability and utility of the sensor image. The results are more pronounced in favor of the LAHE and LABGC techniques, with the impact of the HTC technique being minimal.

4.2 HARDWARE IMPLEMENTATION EVALUATION

This section describes the hardware implementation of each of the image enhancement techniques (LAHE, LABGC, HTC). These mechanizations are constrained to run at real-time TV rates. A functional block diagram of

each technique is given along with an estimate of the number of integrated circuits.

This evaluation concluded that the three enhancement techniques investigated in this study can be mechanized with state-of-the-art hardware. The LABGC and HTC are both much easier to mechanize than the LAHE technique.

To estimate the size, power and weight of each mechanization based on the number of ICs, the following figures were used.

$$\text{Size - Height} = 8''$$
$$\text{Width} = 6''$$
$$\text{Length} = (\text{ICs}) \times 0.02\ ''+2''$$

$$\text{Power} = (\text{ICs}) \times 0.2 \text{ watts}$$
$$\text{Weight} = (\text{ICs}) \times 0.015 \text{ pounds}$$

Table 4-4 summarizes the data collected in this evaluation.

Histogram Equalization

The two dimensional sliding window histogram equalization mechanization is shown in Figure 4-15. It consists of digital memory for the storage of a partial frame of the video plus storage for the histogram itself and special logic to generate the histogram and control the truncation process. Table 4-5 reflects the complexity of this process by defining the number of integrated circuits for the various functions.

TABLE 4-4. SUMMARY OF ENHANCEMENT TECHNIQUES AS TO HARDWARE COMPLEXITY.

Enhancement Technique	Hardware Complexity			
	ICs	Size (Inches)	Weight (Pounds)	Power (Watts)
LABGC	330	6 x 8 x 8.6	5	66
LAHE	770	6 x 8 x 17.4	11.5	154
HTC	384	6 x 8 x 9.7	5.8	77

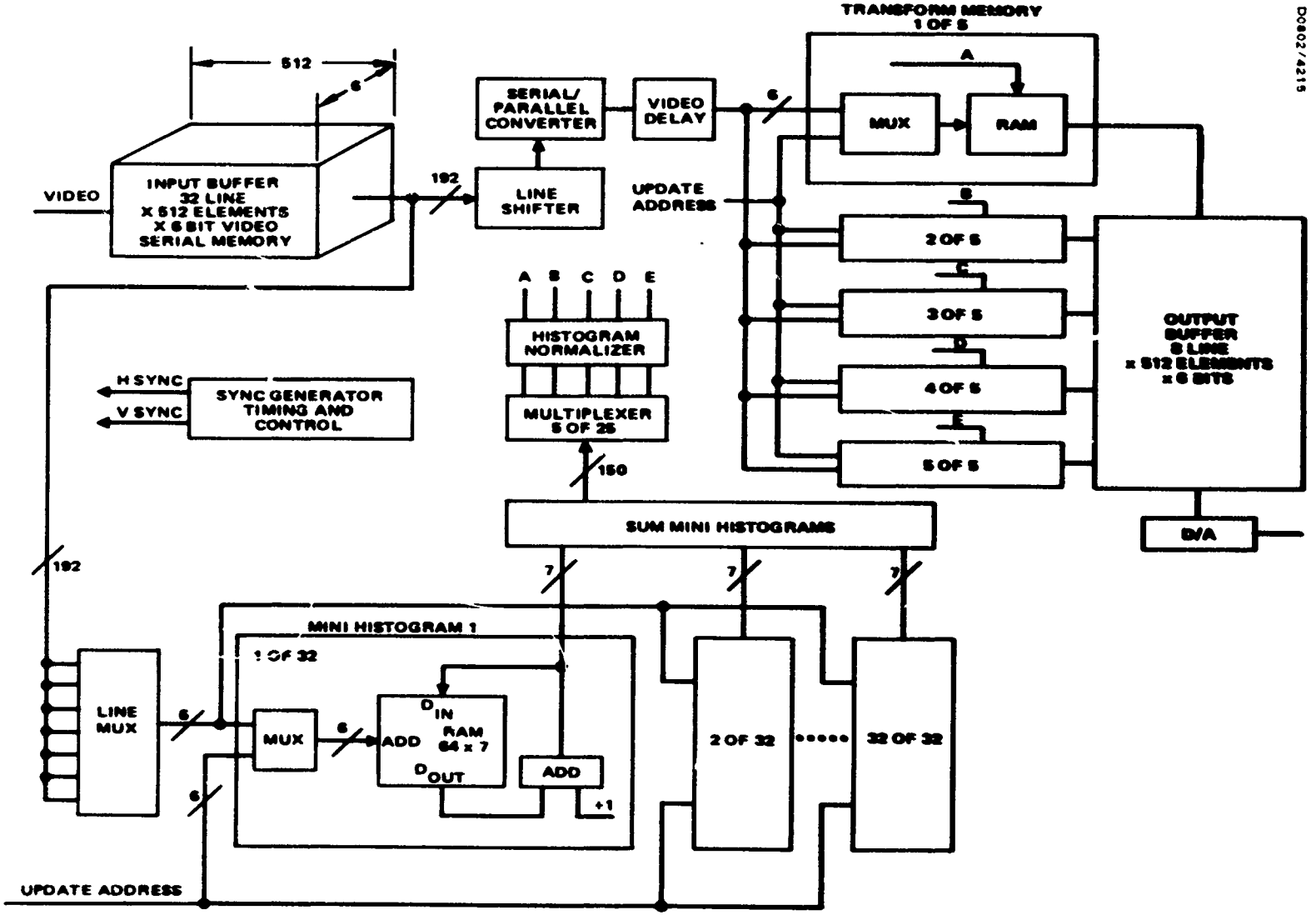

Figure 4-15. Histogram Equalization Block Diagram.

TABLE 4-5. HISTOGRAM EQUALIZATION MECHANIZATION COMPLEXITY

Function	No. ICs
Input Buffer	170
Code Conversion	250
Histogram Storage	150
Output Buffer	100
Timing and Control	100
Total	770

Implementation of the local area histogram equalization algorithm requires 32 lines of video storage to generate the 32 line by 32 element histogram. This 32 x 32 histogram is sub-divided into 8 smaller histograms that are 4 elements by 32 lines called minihistograms. To histogram equalize at TV rates, multiplexing of these histograms is necessary. This minimizes the memory requirements. Each larger histogram of 32 elements by 32 lines is used to equalize the center 4 element by 4 line array. The histogram is then shifted horizontally by 4 elements to convert the next inner 4 x 4 array. Therefore each successive 32 x 32 histogram differs by one 4 x 32 minihistogram. Forming the first histogram requires the summing of 8 minihistograms. Each additional histogram is generated by adding one and subtracting another minihistogram.

Multiplexing of the transform memories is required to allow time to update the transformation data. Since each minihistogram is used in multiple histograms the transform memories must be updated simultaneously. This requires the video conversion process to occur in parallel necessitating a output buffer to convert the timing to standard T. V.

Local Area Brightness and Gain Control

The mechanization of this process as shown in Figure 4-16 consists of memory and processing circuitry to derive the optimum brightness (bias) and gain (contrast) of the video based on its local characteristics. The mechanization complexity estimate is summarized in Table 4-6.

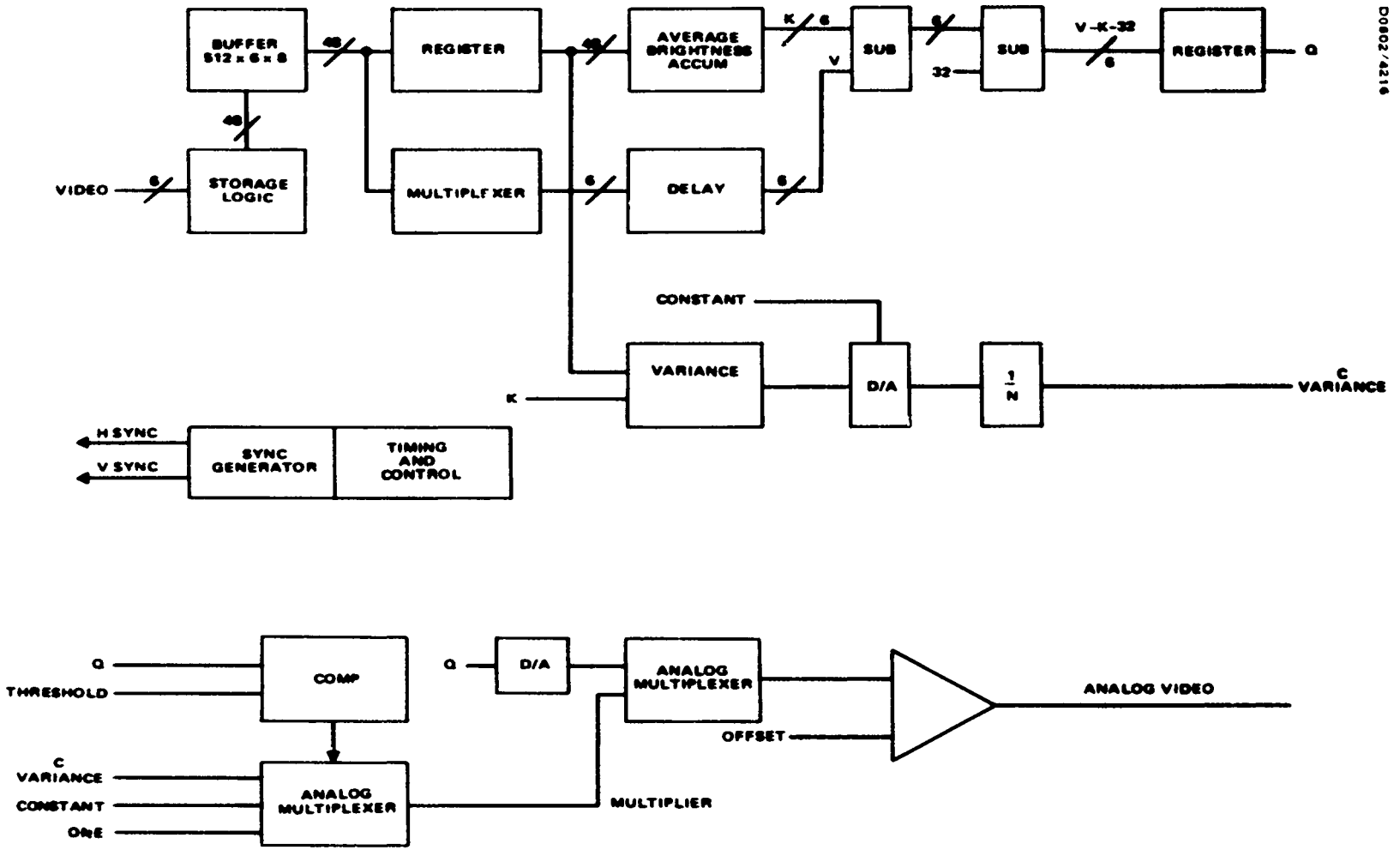

Figure 4-16. LABGC Block Diagram.

TABLE 4-6. LOCAL AREA BRIGHTNESS AND GAIN CONTROL MECHANIZATION COMPLEXITY

Function	No. ICs
Buffer	30
Ave Bright	140
Sync Gen	10
Timing and Control	30
Variance	120
Total	330

The process is implemented by first storing eight lines of video in a recirculating shift register memory. Vertical shifting of the statistical window is accomplished by updating this buffer one line at a time. Horizontal shifting is done by adding the difference between the newest and the oldest video elements to the statistics of the window. The average brightness is then summed over eight lines and subtracted from the center element of the window area.

The video with average brightness removed is digitally multiplied by a gain term. A multiplexer is used to select either a constant gain, or a gain which is inversely proportional to the variance of the statistics. The variance is calculated by the same process as the mean except the video is squared before processing and then subtracted from the mean. The variance calculation is implemented digitally because analog techniques for computing variance for a sliding window of statistics are very complicated.

Haar Transform

The Haar transform mechanization as shown in Figure 4-17, consists of buffer memory for the storage of input digitized video and the intermediate and final transformed results. The actual transform and inverse transforms are performed using high speed arithmetic logic circuits capable of performing the required shifts, adds and subtracts. Table 4-7 reflects the complexity of this approach in terms of the number of integrated circuit components required to mechanize the various functions.

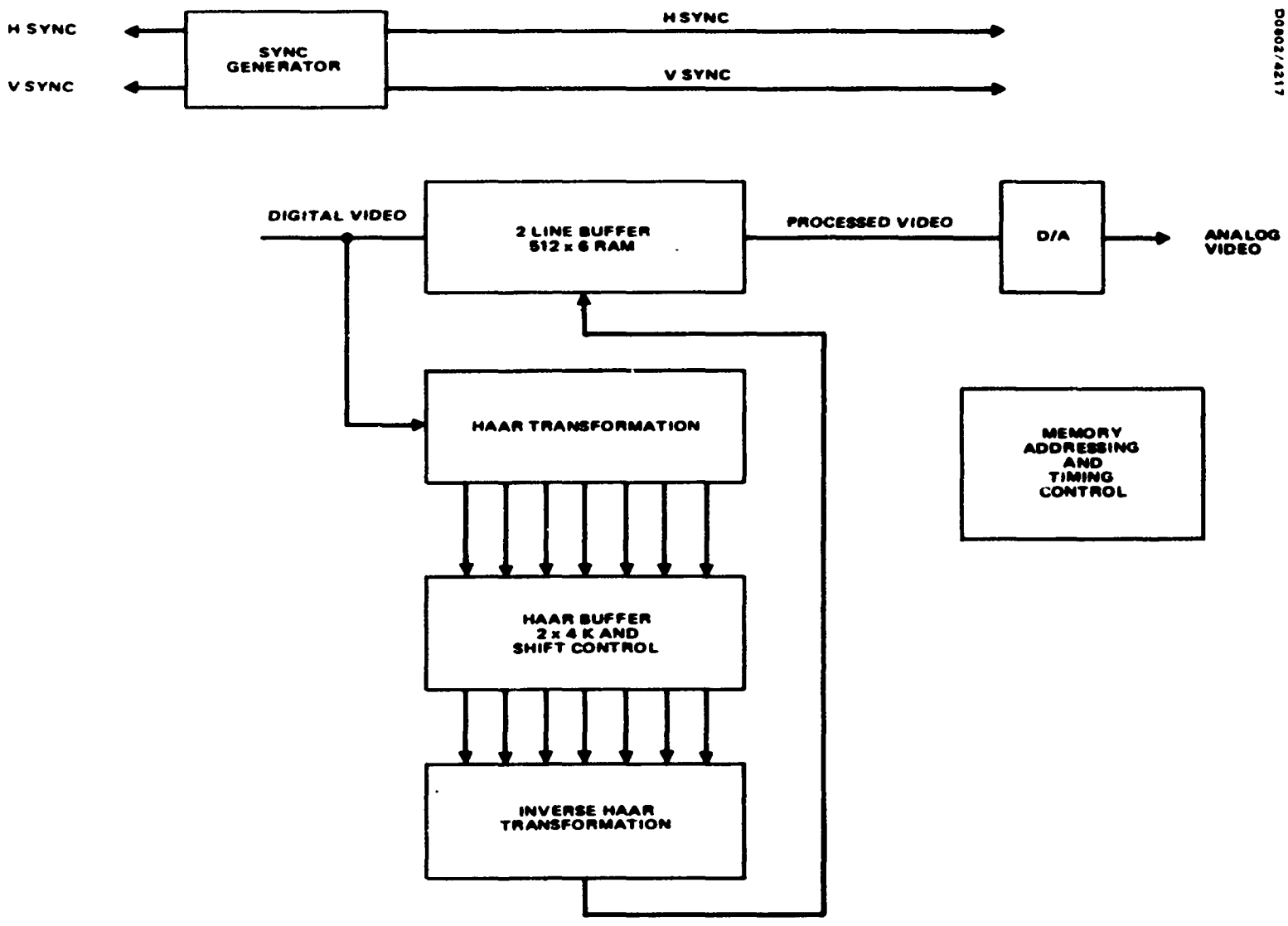

Figure 4-17. Block Diagram Haar Transform.

TABLE 4-7. HAAR MECHANIZATION COMPLEXITY

Function	No. ICs
Sync Gen	10
Input Buffer	12
Haar Xform	137
Xform Buffer	48
Inverse Xform	137
Timing and Control	40
	384

As a line of video is received in the processor, it is stored in the input buffer. The Haar Transform is performed and the transformed data stored in the Haar memory. During the horizontal blanking time the desired shifting function is applied to the transformed video. As the second line of video is received, stored, and transformed, the inverse transformation is performed on the first line and subtracted from the unprocessed stored line in memory. The third line is stored in the first buffer as the first line is being sent to the display.

The Haar transformation is implemented by taking the sum and difference of alternate pixels of video. Difference terms are final terms while sum terms are processed again. Each successive process generates $2^{(8-i)}$ terms where i = 0 to 7. The inverse transformation is identical except the process reverses the order of the sums and differences.

5.0 CONCLUSION

Three image enhancement techniques were investigated, optimized, and evaluated in this study:

1. Local Area Brightness and Gain Control (LABGC),
2. Local Area Histogram Equalication (LAHE), and
3. Haar Transform Crispening (HTC).

The LABGC technique manipulated brightness and gain within local image areas. It was found to work best when the gain was a function of the local standard deviation and the brightness a function of both the local mean and standard deviation. This combination of gain and brightness control produced good enhancements in most cases.

Applying histogram equalization to local image areas, as in the LAHE technique, showed tremendous improvement over the full frame equalization approach. One refinement was made to the LAHE technique. This involved shifting or biasing the mean of the equalized imagery so that it more closely approximated the mean of the unenhanced imagery. This logic was added because in certain cases, histogram equalization biases the enhanced imagery toward the dark end of the intensity scale.

Computer simulations showed that image crispening could be achieved using the Haar transform. Analysis was used to derive a crispening operator composed entirely of binary shifts. This resulted in a technique that produced edge sharpening by a combination of simple addition, subtraction, and binary shifts.

Evaluation

A human factors evaluation of the enhancement techniques was performed. This subjective analysis produced the following conclusions:

1. Viewer acceptance and utility of enhanced imagery is dependent upon the sensor being used, the scene, and the operator task.
2. Enhanced imagery is most useful in detailed interpretation tasks.
3. Enhancement techniques produced the best results with TV type imagery and good results with FLIR scenes.
4. Enhancement techniques are of unknown value when applied to synthetic aperture radar imagery.

This evaluation strongly indicates that image enhancement techniques can be utilized to improve viewer interpretation performance of critical tactical tasks which involve overall target area orientation, target detection, identification and designation. These results are more pronounced in favor of the histogram and LABGC techniques, with the impact of the Haar technique being minimal.

The hardware implementation evaluation indicates that the LABGC and HTC techniques are the easiest to mechanize. The HTC is estimated to be slightly more difficult to mechanize than the LABGC.

In conclusion, this study showed that the LABGC and LAHE techniques can improve operator performance of sensor display systems. This result is very pronounced for electro-optical sensors. The Haar transform crispening technique showed little overall improvement in operator performance. Radar imagery was affected little by enhancement and in some cases actually degraded the image. The LABGC technique is the easiest to mechanize in hardware while the LAHE is the most difficult. Table 5-1 summarizes these results.

FOR THE FUTURE

Future work should be done to optimize the window sizes of both the LABGC and LAHE techniques. Surprisingly, the LABGC technique did slightly better than the LAHE. It was expected that the LAHE technique would do better since it non-linearly reassigns gray scale levels based on image statistics. The LABGC, on the other hand, is a linear technique also

TABLE 5-1. SUMMARY OF ENHANCEMENT TECHNIQUES AS TO IMAGE IMPROVEMENT AND HARDWARE COMPLEXITY.

Enhancement Technique	Average Image Improvement 4.0 = Original	Hardware Complexity			
		ICs	Size (Inches)	Weight (Pounds)	Power (Watts)
LABGC	4.4	330	6x8x8.6	5	66
LAHE	4.3	770	6x8x17.4	11.5	154
HTC	3.85	384	6x8x9.7	5.8	77

using image statistics. However, the extra capability of the LAHE technique to adaptively enhance contrast would seem to have been an advantage. This expectation would most likely be realized with further optimization of window size.

The effects of the enhancements of the radar imagery on operator performance were inconclusive. A possible explanation is that these images were logarithms of the original scenes. This logarithmic process is common in ground mapping radar displays due to the large dynamic range. Applying the enhancement techniques to the original, or linear, radar imagery and evaluation by experienced radar photointerpreters would likely yield improved results.

The Haar transform crispening (HTC) technique didn't perform as well as expected overall. This may have been the result of using fairly crisp images to start with. An investigation of the HTC technique using images that possess real-world blur due to misfocused optics or MTF roll off in the sensor electronics would yield new results. Also, the derivation of a Haar domain crispening operator matched to a specific resolution loss problem, would most likely lead to marked improvement in operator performance. This may in turn permit development of systems in which lower cost and lower quality components can be used with no decrease in performance.

Finally, an evaluation of a selected image enhancement technique should be conducted with real-time man-in-the-loop simulation, or flight tests. This would yield quantitative data on the cost effectiveness of real-time image enhancement techniques for sensor display systems.